The behavior of electricity prices at the German intraday market: A probabilistic functional data approach

Master's Thesis submitted

to

Prof. Dr. Karl Wolfgang Härdle (First Advisor)

Humboldt-Universität zu Berlin

School of Business and Economics

Institute for Statistics and Econometrics

Ladislaus von Bortkiewicz Chair of Statistics

Dr. Błażej Radomski (Second Advisor)

MKonline GmbH

Kurfürstendamm 72, D-10709 Berlin

by

Johannes Stoiber

(564392)

in partial fulfillment of the requirements

for the degree of

Master of Science (Statistics)

Berlin, May 1, 2017

Acknowledgement

I would first like to thank my first thesis advisor Prof. Dr. Karl Wolfgang Härdle of the Ladislaus von Bortkiewicz Chair of Statistics at Humboldt University. During the associated Q-Kolleg he gave valuable comments on my research project and gave me the opportunity to present my master thesis at a workshop at National University of Singapore. I would further like to thank his Ph.D. student Awdesch Melzer for all his support. The door to Awdesch Melzers office was always open whenever I ran into a trouble spot or had a question about my research or writing.

I would further like to thank my second thesis advisor Dr. Błażej Radomski and the team of MKonline in the Berlin office. They supported me during my master thesis with valuable comments and constructive discussions about the electricity market. I would further like to thank MKonline for providing the data for my research project.

Finally, I must express my very profound gratitude to my parents and to my girlfriend for providing me with unfailing support and continuous encouragement throughout my years of study and through the process of researching and writing this thesis. This accomplishment would not have been possible without them.

Abstract

Increasing renewable energy sources, such as solar and wind pass uncertain weather conditions to uncertainty in power production. This requires market participants to react at short notice to fulfill closed contracts through balancing themselves at the intraday market. Prices at the German intraday market correlate inter- and intradaily and exhibit extreme values in both directions. As a result of such extreme movements, interest on future prices is not only in the center of the distribution, but also in the tails. Generalized quantiles such as quantiles and expectiles are well suited to characterize a distribution. This thesis shows an application of two approaches to identify main risk factors of generalized quantile curves. Functional principal component analysis and a multivariate factorisable quantile regression. The interdaily time dynamics of the risk factors are analyzed with a vector autoregressive model that allows for incorporation of exogenous information such as renewable energy production forecasts. Price forecasts from both models are evaluated with root mean squared error and mean absolute error. Intervals obtained from tail forecasts are evaluated, to which share the interval captures observed prices. Supplementary material for this thesis is available via QuantNet on GitHub.

Keywords: Expectiles, FASTEC, FPCA, Functional time series, High-dimensional data analysis, Intraday market for electricity, Multivariate quantile regression, Short term energy price forecasting, SVD, VWAP

Zusammenfassung

Der Anstieg an Energieerzeugung durch erneuerbare Energien wie Solar und Wind führen dazu, dass unsichere Wetterbedingungen zu Unsicherheiten bei der Stromproduktion führen. Daher müssen Marktteilnehmer kurzfristig reagieren könne um abgeschlossene Verträge einhalten zu können. Eine Plattform dafür bietet der Intraday Markt. Preise am deutschen Intraday Markt korrelieren inter- und intratäglich und weisen sowohl negative als auch positive Extrempreise auf. Aufgrund solcher Extrempreise liegt das Interesse bezüglich Preisprognosen nicht nur im bedingen Mittelwert sondern auch in den Verteilungsenden. Generalisierte Quantile wie Quantile und Expectile eignen sich gut um eine Verteilung zu beschreiben. Diese Arbeit zeigt die Anwendungen von zwei Methoden zur Identifizierung von Risikofaktoren von generalisierten Quantilskurven von Strompreisen am Intraday Markt. Die Risikofaktoren werden durch Funktionale Hauptkomponentenanalyse und Multivariate Quantilsregression identifiziert. Die intertägliche Dynamik der Risikofaktoren wird mit einem Vektorautoregressiven Modell analysiert. Dadurch können auch exogene Informationen wie Prognosen über erneuerbare Energieproduktion berücksichtigt werden. Preisprognosen beider Ansätze werden evaluiert mithilfe der Wurzel der mittleren quadratischen Fehler. Aus den Prognosen der Verteilungsenden werden Intervalle berechnet. Diese werden dahingehend evaluiert, zu welchem Anteil sich Preise innerhalb des Prognostizierten Intervalls befinden. R-Codes werden via QuantNet auf GitHub zur Verfügung gestellt.

Schlagwörter: Expektile, Funktionale Hauptkomponentenanalyse, Funktionale Zeitreihen, Hochdimensionale Datenanalyse, Intraday Markt für Strompreise, Multivariate Quantilsregression, kurzfristige Strompreisprognosen, Singulärwertzerlegung, Volumen gewichteted Durchschnittspreise

Contents

List of Abbreviations

act	actual observed data
ADF	Augmented-Dickey-Fuller
AIC	Akaike information criteria
BIC	Bayesian information criteria
CDF	cumulative distribution function
DAspot	price according to day-ahead auction
df	degrees of freedom
EEX	European Energy Exchange
EPEX Spot	European Power Exchange
FASTEC	factorisable sparse tail event curves
FDA	functional data analysis
FIC	forecast interval coverage
FISTA	fast iterative shrinkage-thresholding algorithm
FPCA	functional principal components analysis
FPC	functional principal component
IER	inter expectile range
IQR	inter quartile range
KH	Karhuhen-Loève
KPSS	Kwiatkowski-Phillips-Schmidt-Shin
MAE	mean absolute error
mk	MKonline forecasted data
MQR	multivariate quantile regression
PCA	principal component analysis
PC	principal component
RL	residual load
RMSE	root mean squared error
SVD	singular value decomposition
TSO	transmission system operator
VAR	vector autoregressive
VARX	vector autoregressive with exogenous variables
VWAP	volume weighted average price

List of Figures

List of Tables

1 Introduction

During the past decades energy markets have undergone substantial changes. The liberalization in Germany in the late 1990s unbundled a highly vertical integrated market and transformed it into a deregulated competitive one. Market participants are now generators, distribution companies, traders and large consumers who interact bilateral or through the European Power Exchange (EPEX Spot). A further disruption of the German market has been triggered by the *Energieeinspeisegesetz* in 1991, a feed-in tariff that guarantees grid access for renewable energy sources. Most important sources are solar SPV and wind. In 2015 energy from these two sources covered with 115.583 produced TWh 19.4% of German energy consumption (BMWi 2017). For the remainder in this thesis the term renewable energy refers to solar and wind energy production and neglects other sources like hydro.

The rise of weather dependent energy generators is associated with uncertainty in power production. Planned production and consumption are primarily traded at least one day before physical delivery. One day before delivery, there is an auction for all contracts at the following day (day-ahead auction). However, actual load production or consumption may deviate from the committed ones. Take as an example a day with unexpected blazing hot sunshine. On the one hand, solar production will be higher than the committed one. On the other hand, people may go out and enjoy the sun, turn off electronic devices and reduce heating. As long as there is no heat wave and people do not turn on air conditioners, more energy would be available and less energy would be demanded at this day. Since energy is not storable (in relevant quantities), demand and consumption need to be balanced at all time to maintain grid stability. Hence traders have to adjust their portfolio at all time. Such short term adjustments can be executed at the continuous intraday market at EPEX Spot up to 30 minutes before physical delivery. Trading short term until delivery allows to take more recent production forecasts into account which exhibit increasing accuracy as time of delivery approaches (Holttinen 2005). The importance of intraday trading is also pointed out by Bueno-Lorenzo et al. (2013) with an example about Spanish electricity prices. Prices at the German intraday market have been minor subject to literature. Some researcher investigate order book data and bidding strategies (see e.g., Garnier & Madlener (2015) or Kiesel & Paraschiv (2017)) and others focus on forecast errors concerning consumption and renewable production.

Hagemann (2015) applies a multiple linear regression model in order to relate deviation between intraday and day-ahead prices with supply variables such as generator outages,

renewable forecast errors and net imports from France. While the models confirm the impact of dependent variables at reasonable significance levels, their poor overall fit with an adjusted R^2 of 0.19 and 0.22 makes the models impractical for predictions. Pape et al. (2016) are able to explain about 75% of variation in intraday prices with a root mean squared error (RMSE) of 9.7 for the years 2012 to 2013 with a fundamental model approach. Fundamental models explain the price as a result of a market equilibrium where demand meets supply and incorporate economic fundamentals such as renewable production, total demand, prices for fuel or CO_2, generator outages etc. as exogenous variables (see e.g., Mount et al. (2006)). A contour plot is used by v. Selasinsky (2016) to visualizes forecast errors of residual load and deviation between intraday and day-ahead prices. The term residual load refers to the difference between energy consumption and renewable infeed. He further runs a simulation on the costs for balancing renewable forecast errors in the intraday market. This thesis analyzes the behavior of electricity prices at the German intraday market.

Residual load is the amount of energy produced by conventional energy sources such as nuclear, coal, lignite, oil and gas. These sources exhibit higher marginal costs of generation than renewable energy sources which operate at almost zero marginal costs. Therefore prices tend to be lower in times of high renewable infeed (see e.g., Nicolosi (2010) or Cabrera & Schulz (2016)). This relation is known as merit-order effect and is discussed intensively in literature (see e.g., Ketterer (2014) or Würzburg et al. (2013)). Increasing renewable capacities lead to high residual load volatility that translates into volatility and extreme spikes for electricity prices in Germany (Mayer 2014). In a recent analysis of German and Danish electricity prices, Rintamäki et al. (2017) find out that wind energy increased price volatility in Germany, but they observe the opposite for Denmark. In a competitive environment as it is the case for the German energy market, price forecasts are crucial for generators, traders and large consumer in order to maximize their profits. In a comprehensive survey on electricity prices, Weron (2014) points out the need for probabilistic forecasts of electricity prices. He states that because of extreme prices, market participants are not only interested in point forecasts but also in the dispersion of future prices. Probabilistic forecasts refer to the prediction of intervals and distribution of future realizations of a random variable. These techniques have drawn much attention within the past years as reported by Gooijer & Hyndman (2006), but literature on probabilistic electricity price forecasting is scarce (Weron 2014). Amjady & Hemmati (2006) argue that high-quality prediction intervals for the market clearing electricity prices may be a helpful tool to reduce risk in bidding strategies. Serinaldi

(2011) models the distributional parameters location, scale and shape for short term forecasts with a generalized additive model. In a recent survey on prices in Denmark Jónsson et al. (2014) use quantile regression to describe the density between 5% and the 95% quantiles and approximate the tails with an exponential distribution. Bello et al. (2016) establish probabilistic medium-term price forecasts for the Spanish market based on a fundamental model combined with spatial interpolation techniques. The Spanish market is also investigated by Moreira et al. (2016) who provide probabilistic forecasts for day-ahead prices in 5% steps from 5% to 95% quantiles. Nowotarski & Weron (2015) compute prediction intervals for day-ahead prices in North America with quantile regression averaging. Cabrera & Schulz (2016) apply a functional kernel density estimation conditional on residual load in order to obtain electricity price density forecasts for Germany. They show further how the estimated price densities can be used to derive risk measures such as Value-at-Risk and Expected Shortfall. In this thesis two models based on functional data are applied to produce probabilistic forecasts of German intraday prices.

Generalized quantiles such as quantiles (Koenker & Bassett 1978) and expectiles (Newey & Powell 1987) are well suited to describe distributional characteristics. Both measures depend on an asymmetry parameter $\tau \in (0, 1)$ which describes a certain part of the distribution. While $\tau = 0.50$ represents the center of the distribution, values of τ close to 0 and 1 describe the tails of the distribution. An inherent feature of electricity data is that they are observed and available in equispaced intervals e.g., 24 hours a day, 365 days a year without breaks on weekend or bank holiday. This distinguishes them from financial time series such as stock prices or returns and one can apply statistical tools as they are meant to be used (Weron 2006). As a consequence electricity prices can be treated as univariate but also as multivariate time series. In this thesis daily price curves are regarded as realizations of a functional time series. An observation of the functional time series refers to a specific day and represents the intradaily curve as a function. An introduction to functional data analysis (FDA) is provided by Ramsay & Silverman (2005) and for the theoretical framework of FDA refer to Eubank & Hsing (2015).

This thesis demonstrates the application of two FDA models to reduce the dimensions of the intraday electricity price curves. The first approach is based on Functional Principal Component Analysis (FPCA), a common tool to reduce dimensions of functional data. There is a vast amount of FDA literature on load demand (e.g., Ferraty & Vieu (2006), Antoch et al. (2010) or Cabrera & Schulz (in press)). For electricity price data the contrary is the

case. Vilar et al. (2012) provide load and price forecasts using a nonparametric functional regression approach. The functional factor model by Liebl (2013) decomposes nonparametric price-demand functions at the German day-ahead market with FPCA. In a recent survey Aneiros et al. (2016) present a robust FPCA technique that uses functional data as response and explanatory variable for the Spain market. An adaptive functional autoregressive forecast model is developed by Chen & Li (2015) and applied to electricity prices in California. The FPCA model in this thesis follows the methodology of Cabrera & Schulz (in press). In a first step, nonparametric expectile curves are jointly estimated for each day for τ levels of interest. Then FPCA is applied to the daily curves for each τ level. As a result common factors are obtained providing time series of factor scores that correspond to a certain asymmetry parameter τ. Factors are selected such that at least 95% of variation of the respective τ expectile is explained. The second approach is the application of the factorisable sparse tail event curve (FASTEC) model, proposed by Chao et al. (2015). The term FASTEC refers to a multivariate quantile regression (MQR) with reduced rank. It is designed to deal with extreme quantiles, i.e., tails and is applicable to functional data. Generalized quantile curves for a certain asymmetry parameter are estimated jointly for all days and risk factors are simultaneously obtained through singular value decomposition (SVD) of the coefficient matrix. To the best knowledge of the author, this thesis shows a first application of the model from Chao et al. (2015) to produce probabilistic forecasts of electricity price curves.

Both models deliver for each day and each τ generalized quantile a vector of factor scores/loadings. These are analyzed with a vector autoregressive (VAR) model as presented in Lütkepohl (2005). This model allows to incorporate exogenous information such as residual load and prices from the day-ahead auction.

The approach presented in this thesis provides forecasts of the dispersion of future electricity prices based on FDA. The inter- and intradaily dependency structure of those prices is taken into account and probabilistic estimates of common factors are obtained through the FPCA and FASTEC model. The presented strategy is flexible in a sense that it allows inclusion of exogenous information and one does not rely on distributional assumptions. The methods are applied to volume weighted average prices (VWAP) from the German intraday market. It turns out that the FASTEC model provides more reasonable interval forecasts then the FPCA model. The forecasted intervals between the 1% and 99% quantile capture almost 80% of observed prices, using day-ahead prices as exogenous information. If the interest is only in point forecasts the FPCA model outperforms the FASTEC model. However

the day-ahead prices provide even better point forecast in terms of RMSE.

The remainder of this thesis is organized as follows. The next section gives an overview of the short term electricity market in Germany and presents the data for the empirical analysis. The empirical strategy is described in section (3). The application to the data is provided in section (4) and section (5) concludes.

2 Short term power market in Germany

This section provides an overview of the German short term power market. At first the market structure is explained taking into account generation, transmission and trading of electricity. This will be followed by a description and summary statistics of the used data. The data is provided by MKonline, an analysis service for the European power market (MKonline 2017).

2.1 Market structure

Liberalization of European electricity markets has been initialized in 1997 with the Directive 96/92/EC. The directive aimed to break monopoly structure of the highly vertically integrated electricity markets in Europe. Highly integrated in this context means that a single energy company provides the whole value chain from generation of energy to transmission and distribution right up to retailing for a certain area. The directive further intended to form a common European energy market with higher energy efficiency and lower consumer prices. Two decades later European markets have changed fundamentally. The vertical integrated market structure does not exist anymore. In Germany the grid has been outsourced and is now operated by four transmission system operators (TSOs). These are TransnetBW, Tennet TSO, Amprion and 50Hertz Transmission. They are responsible for a grid frequency of 50 hertz. Since electricity is not storable in huge quantities, consumption has to be balanced continuously against demand in order to keep the system stable. For this reason technical markets such as balancing or ancillary markets provide a last resort to manage grid stability. For more information about technical markets see e.g., Farahmand & Doorman (2012), Just (2015), Müsgens et al. (2014) or Riedel & Weigt (2007). In contrast to these purely physical markets, wholesale electricity markets offer a marketplace for short and long term physical and financial products. Since the focus of this thesis is on physical products, financial derivatives such as futures, swaps and options are not covered here. Standardized short term products can be traded at EPEX Spot which operates a day-ahead and intraday market. For more information on EPEX Spot day-ahead auction refer to EPEX Spot (2017*a*) and for the intraday market to EPEX Spot (2017*c*). Both markets provide trading of 15-minute, hourly and block contracts with physical delivery. Block contracts refer to a bunch of hours, most important are those for base (00:00 - 24:00) and peak (08:00 - 20:00). The features of both markets are described below and refer to hourly contracts including those for blocks. The market design for 15-minute and the recently introduced 30-minute intraday market is quite similar except some minor differences. Short term contracts can also be traded bilateral over-

the-counter. However, prices should not differ that much to those at EPEX Spot, otherwise arbitrage would be possible (Nicolosi 2010).

The day-ahead market. The price building mechanism for hourly products at the day-ahead market is conducted through an auction. Participating agents submit supply and demand bids containing information about quantity, price and delivery period on the following day to EPEX Spot. The minimum volume is 0.1 MW and prices are allowed to range between -500 EUR/MWh and $3,000$ EUR/MWh with a minimum increment of 0.1 EUR/MWh. Bids can be submitted to EPEX Spot until the auction takes place at 12:00 noon every day, including weekend and public holidays. Prices and volumes are determined through the merit order. That means generators are ordered by their marginal costs. Hence, they represent an increasing supply curve. The last (supply) offer that is able to satisfy requested load for a certain price is the so called merit order and determines price and volume for a specific contract. The outcome of the auction is published at 12:40 noon by EPEX Spot.

The intraday market. The intraday market for hourly contracts at EPEX Spot is organized as a continuous trading market. Such a market design is frequently observed in most exchanges e.g., for stocks or derivatives. Intraday trading at EPEX Spot starts each day at 15:00 for contracts with physical delivery on the following day. Each contract can be bought and sold throughout until 30 minutes before delivery. Hence, traders are more flexible regarding trading time compared to the day-ahead auction. Similar to the bidding mechanism at the day-ahead market, players submit buy or sell orders for a certain contract with information about volume and price to EPEX Spot. Minimum trading volume is 0.1 MW and prices are restricted between $-9,999$ EUR/MWh and $9,999$ EUR/MWh, with an increment of at least 0.1 EUR/MWh. All these bids are then listed in the order book. First they are prioritized by price. This means that buy orders are sorted descending and sell orders in an ascending order. As a result the two orders with the smallest price spread are on top of the book. Execution is conducted as soon as possible. In case of competing orders, the order which has been submitted earlier is executed.

Both markets at the EPEX Spot play an important role to cope with challenges that arise from the expansion of renewable energy production. Expected renewable production can be traded through the day-ahead auction and give an idea about the level of renewable infeed on the next day. The intraday market allows flexible short term adjustments and portfolio balancing when renewable production forecasts become more accurate as time of delivery approaches (Holttinen 2005). Forecast errors are mainly an issue for renewable energy pro-

duction. Nevertheless, unforeseen outages between day-ahead closure and fulfillment may be an issue for conventional power producers. These outages only impact the production schedule if the respective generator has been dispatched at the day-ahead settlement (Hagemann 2015). But also consumers may be facing unforeseen changes and demand more or less electricity power as they have bought at the day-ahead auction. Market participants who are hit by such forecast errors can balance themselves at the intraday market. Remaining imbalances after the intraday trading closes are then balanced by the TSOs, which draw on control energy to maintain grid stability. Agents that utilize such TSO services are charged ex-post. However, players should not rely on these services and balance themselves. TSO balancing services in Germany are more expensive than the intraday market and TSOs can terminate balancing contracts with market participants who use these services for too many times (Pape et al. 2016). Therefore the rise of intermittent renewable energy sources in Germany emphasizes the relevance of the intraday market since it enables self-balancing and short term adjustments of weather independent generators to ensure an equilibrium between supply and demand (Bueno-Lorenzo et al. 2013). This helps to maintain grid stability and preserves market participants from expensive imbalance services.

2.2 Electricity market data

The data for the empirical analysis in this thesis is provided by MKonline, an analysis service for the European power market (MKonline 2017). They set up forecasts regarding load demand, renewable energy production and electricity prices for short-, mid- and long-term horizon. MKonline provides these forecasts as well as actual data for most European countries. Actual data is provided by MKonline as a third-party vendor. All time series that are used in this thesis are queried in hourly resolution for the period from 2014-01-01 to 2016-12-31. In total, each series has a length of $26,304$ observations. In order to distinguish between actual (act) and forecasted data from MKonline (mk), time series are supplemented by act or mk. Prices from the day-ahead auction are denoted by DAspot. Table (1) provides summary statistics of the used time series. Power production data is presented in GWh and prices are given in EUR/MWh.

The VWAP series is originally obtained from EPEX Spot and does not contain cross-trades. Cross-trades are buy and sell orders from the same trader that net out each other. Imagine a portfolio manager who operates a wind park in the northern sea and a solar park in Bavaria. Say that he he sells 10 MW for the hour 10:00 - 11:00 for 20 EUR per MW in

order to balance his wind park and fulfill his delivery commitments. Assume further that the weather has changed in Bavaria and the manager also needs to take care for the solar park. For this reason he buys 10 MW for the hour 10:00 - 11:00 for the same price at the same time. Since the activities from this trader net out each other, they are not taken into account for computation of the VWAP. The VWAP series contains one missing observation. On 2014-03-13 the 19:00 contract (contract for delivery period 19:00 - 20:00) has not been traded at all at the continuous intraday market. It seems reasonable to assume that there had been no forecast errors from renewable production that had to be balanced at the intraday market. Therefore the missing value is replaced by the DAspot for the 19:00 contract. The price series from the day-ahead auction is also originally provided by EPEX Spot.

Actual wind and solar infeed data is provided to MKonline by the European Energy Exchange (EEX) separately for each of the four TSO areas. Missing values are treated on TSO level. Those that did not stem from time changes could be found either on the EEX or TSO website. Missing values from time changes are replaced by the mean of the surrounding hours for wind data and by zero for solar infeed since there is no sunshine at night. After taking care for the missing values on TSO level, data for renewable energy production is aggregated for whole Germany and one obtains actual wind and solar data. ENTSO-E transparency provides MKonline with time series on hourly load consumption. Since validated actual consumption data is available with a delayed period, MKonline adjusts data that had not been validated with an internal model. Missing values regarding actual consumption are replaced by the mean of the same hour at the same weekday one week before and after. The goal of this thesis is to produce forecasts for the VWAP series. Hence, actual data would not be available in a real world application. Nevertheless, they may provide useful information about their impact on the VWAP series. For practical implementation, one has to draw on forecasts. MKonline provides the most recent forecasts before the day-ahead auction takes place.

Table (1) shows that both, actual and forecasted solar and wind production series have higher mean than median, as it is the case for right skewed series. Indeed, these four series are skewed to the right with skewness ranging between 1.33 and 1.53. Renewable production exhibits high variation and also periods are observed where production is close to zero or even zero. This is not surprising for solar energy, because there is no sunshine at night to produce solar power. This is also the reason, why mean and median deviate that strong for solar power. Wind power depends strongly on wind speed, hence if wind speed is very low, almost no wind power is produced. This explains very low observations of wind power. Both price

Time Series	Mean	Median	SD	Min	Max	Skewness
Consumption (act)	59.05	58.76	10.35	33.72	85.29	−0.01
Solar (act)	3.89	0.14	5.91	0	26.06	1.53
Wind (act)	7.86	5.81	6.68	0.03	33.63	1.33
Consumption (mk)	58.44	58.08	10.28	30.49	80.75	−0.02
Solar (mk)	3.94	0.20	5.85	0	26.78	1.44
Wind (mk)	7.57	5.51	6.51	0.17	34.80	1.49
DAspot	31.12	30.23	12.74	−130.09	104.96	−0.33
VWAP	31.29	30.66	13.84	−161.11	140.60	−0.41

Table 1: Summary statistics. Actual and forecasted time series for consumption, solar and wind energy in GW. Time series for the prices in EUR/MWh.

VWAP_Descriptive

series show a slight skewness to the left, as well as extreme values. The VWAPs ranges from −161.11 EUR to 140.60 EUR within the three observed years. These values are more extreme in both directions than the DAspot which ranges in the same period between −130.09 EUR and 104.96 EUR. The VWAP series further displays higher mean, median and volatility than prices from the day-ahead auction. A reason for negative prices are renewable energy sources with guaranteed feed-in tariffs. This means that all energy produced by renewable energy sources is fed into the grid and conventional generators are pushed into the background. Adjustments of power plants like nuclear or lignite are only possible up to some extent and very slow. Such inflexible producers prefer in some situation to pay consumers for using electricity instead of turning off a generator for a short period.

The polygon plot in figure (1) illustrates actual energy consumption and production sources on two distinct days. The overall consumption is described by the uppermost line. The yellow, green and brown shaded areas represent solar, wind and residual load production. The days are different with respect to three characteristics. First, there is a considerable difference in overall consumption between summer and winter. In general, energy consumption during winter is higher than in summer. Demand for heat in households and offices is much lower in summer, which explains the lower overall consumption to some extent. Second, one has to take into account that 2014-01-21 is a Tuesday and the 2016-05-08 is a Sunday. The shape of the overall consumption on the Tuesday is representative for a business day. One observes a steep increase in the morning hours when people get up and go to their offices. During the working day power consumption remains on a certain level and goes down in the

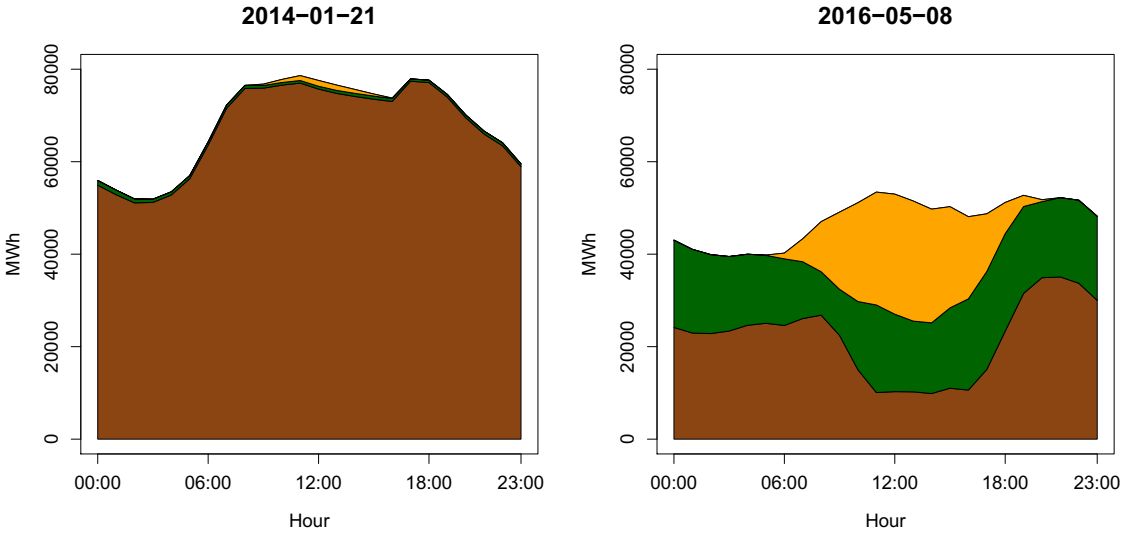

Figure 1: Total load consumption as accumulation of solar infeed (yellow), wind infeed (green) and residual laod (brown) on a day with low (left) and high (right) renewable infeed.

VWAP_Polygonplot

evening hours. During night when people sleep and industrial production is not that high, energy consumption is low. The shape of the overall consumption on a Sunday is distinct from that to a business day as illustrated in the right graph. The overall level is lower since load demand is in general lower on a Sunday. Note further, that the increase during the daylight hours is much less steep than on a business day. Third, there is a significant difference in renewable energy infeed. The winter day on 2014-01-21 displays high overall demand and low renewable energy production. On 2016-05-08 the contrary is the case and residual load is exceedingly low on that day. Marginal energy production costs for residual load are higher than those for renewable energy sources and increase with the level of residual load. As a consequence, DAspot and VWAP are on 2014-01-21 considerable above their averages during peak hours. The high share of renewable infeed on 2016-05-08 leads to extreme prices for both series. Both price series unveil their absolute minimum value during the observed period for the 14:00 contract on 2016-05-08 with -161.11 EUR and -130.09 EUR as given in table (1). As residual load compromise information about location in the merit order curve, actual (RLact) and forecasted values for residual load (RLmk) as well the corresponding forecast error (RLdiff) are used as explanatory variables. For the analysis in this thesis, residual load is computed as difference between energy consumption and renewable infeed. Since prices from the day-ahead auction are available and contain information on the location in the merit

order, DAspot is also used as explanatory variable. Table (2) gives information on correlation among the variables. While RLdiff shows almost no correlation with the VWAP series, the others series correlate quite strong with VWAPs.

	VWAP	RLact	RLmk	RLdiff	DAspot
VWAP	1	0.783	0.801	−0.024	0.891
RLact	-	1	0.961	0.187	0.860
RLmk	-	–	1	−0.092	0.849
RLdiff	-	–	–	1	0.080
DAspot	-	–	–	–	1

Table 2: Correlation of variables.

Figure (2) displays the VWAP series according to its two dimensions. One dimension is regarding the hours within one day and the second illustrates the days. The figure depicts further the daily and yearly seasonality. The seasonal behavior is interrupted by extreme prices. As an example, the extreme negative price of −161.11 EUR on 2016-05-08 is clearly visible as low point in the orange shaded price curve.

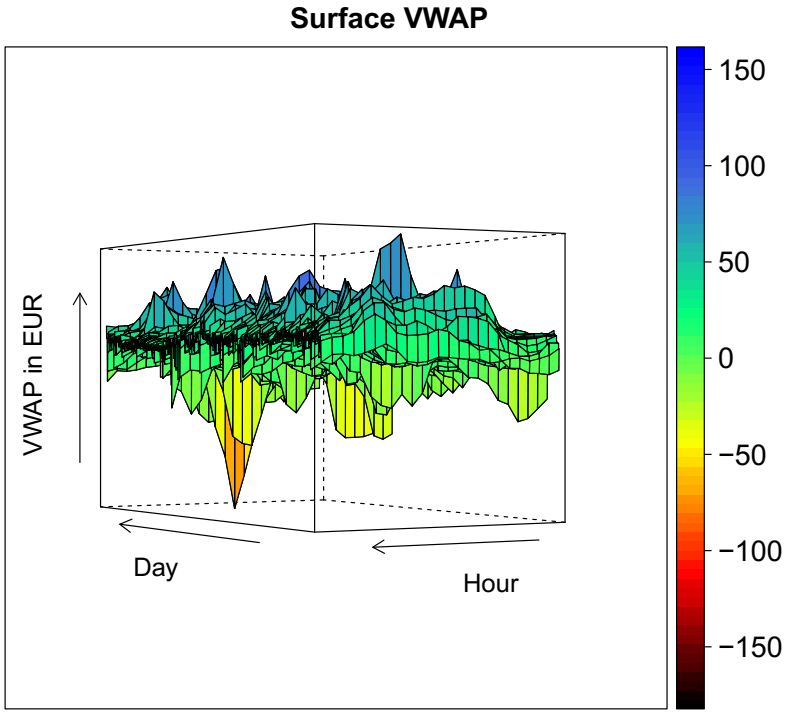

Figure 2: Daily VWAP curves from 2014-01-01 to 2016-12-31. Colors indicate price level.

VWAP_Surfaceplot

3 The model

This section describes the empirical strategy and explains how probabilistic forecasts are obtained. First, the series is deseasonalized taking weekly and yearly seasonal patterns into account. In a second step, the concept of generalized quantiles is explained. This is followed by a presentation of the applied functional data models, the FPCA model and the FASTEC model. Both models reduce the dimensions and identify main risk factors of the daily VWAP curves. Finally, it is described how the time dynamics of the factors can be forecasted with a VAR model.

3.1 Seasonal effects

The seasonal pattern of the VWAP series can be modeled deterministically. Therefore the observed VWAP is expressed as

$$\widetilde{P}_s = \Lambda_s + P_s, \tag{1}$$

where $s = 1, \ldots, S$ represents the hourly observations of the time series, Λ_s describes the deterministic (seasonal) component and P_s the stochastic component. The deterministic component is modeled as a sinusoidal wave as suggested by Weron (2006) and extended such that different weekdays and public holidays are taken into account. Such an approach is also applied by Cabrera & Schulz (in press) for load analysis. The deterministic element is estimated with an ordinary least squares regression separately for each hour $t = 1, \ldots, T$ as follows:

$$\begin{aligned}\Lambda_{t,j} = a_t + b_t \cdot j + \sum_{i=1}^{6} day_{i,t} \cdot DAY_{i,j} + \sum_{k=1}^{5} ph_{k,t} \cdot PH_{k,j} + \\ + \sum_{q=1}^{4} c_{q,t} \cdot \sin\left(\frac{2\pi j}{365}\right) + \sum_{p=1}^{4} d_{p,t} \cdot \cos\left(\frac{2\pi j}{365}\right),\end{aligned} \tag{2}$$

where $j = 1, \ldots, J$ describes the respective day and $T \cdot J = S$. The coefficients a_t, b_t, $c_{q,t}$, $d_{p,t}$, $day_{i,t}$ and $ph_{k,t}$ with $q = p = 1, \ldots, 4$, $i = 1, \ldots, 6$ and $k = 1, \ldots, 5$ are estimated. The dummy variables for six weekdays are given by $DAY_{i,j}$ and those for public holidays by $PH_{k,j}$. MKonline determines public holiday effects on load demand. Based on these estimates, affected days are divided into five categories depending on the intensity of the determined holiday effect. The impact of public holidays on load demand depends if the holiday applies to entire Germany or only to some federal states. Further the impact differs if the public holiday takes place on a business day or on the weekend. So called *bridge*

days, which are single days between a public holiday and the weekend as well as Christmas holidays also have an impact on energy demand. The specifications of the five categories and the corresponding days are summarized in Appendix (A).

The VWAP time series consists of two time dimensions, days and hours as illustrated in figure (2). Hence, the data can be reorganized in a panel structure of dimension $(T \times J)$. This means that the deseasonalized VWAP series P_s can be split into daily curves with T observations and is henceforth denoted by $\mathbf{P} = (P_{t,j}) \in \mathbb{R}^{T \times J}$ where t refers to a certain hour and j marks a certain day. The timings of measurement t are identical for all j. The deseasonalized VWAP curve for day j is given by $P_{*j} = (P_{1,j}, \ldots, P_{T,j})^\top \in \mathbb{R}^T$, the jth column vector of $\mathbf{P}$.

3.2 Generalized quantiles

This subsection first provides an explanation for the term quantile in a univariate setting. This is then extended to conditional quantiles and finally to conditional generalized quantiles. Quantiles are usually found by sorting and ordering observations from a sample. A quantile q^τ, with $\tau \in (0, 1)$, is a statistical parameter that divides the distribution of a sample into two parts. The share of observations lower or equal q^τ is τ, the remainder of the sample is higher than q^τ and has a share of $(1 - \tau)$. Therefore quantiles are well suited to characterize the distribution of a sample. For any random variable $Y \in \mathbb{R}$ with a cumulative distribution function (CDF) $F(y) = P(Y \leq y)$ the τ-quantile is defined as the inverse of the CDF given by

$$q^\tau = F^{-1}(\tau) = \inf\{y : F(y) \leq \tau\}. \tag{3}$$

A general approach to identify a certain quantile that does not rely on sorting and ordering data is obtained through the loss function

$$\rho_\tau(u) = u\{\tau - \mathbf{I}_{(u<0)}\}. \tag{4}$$

Where $\mathbf{I}_{(\cdot)}$ is an indicator function with output 1 if $u < 0$ and 0 otherwise. A graphical illustration of $\rho_\tau(u)$ is given in figure (3). The loss function is in general asymmetric (Koenker 2005). The underlying idea of this loss function is to *penalize* positive and negative residuals u differently. A symmetric exception is given for $\tau = 0.50$ which refers to the median. The quantile function for a certain τ is then the solution to the minimization problem for the expected loss of $Y - \theta$:

$$q^\tau = \arg\min_{\theta \in \Theta} \mathrm{E}\{\rho_\tau(Y - \theta)\}. \tag{5}$$

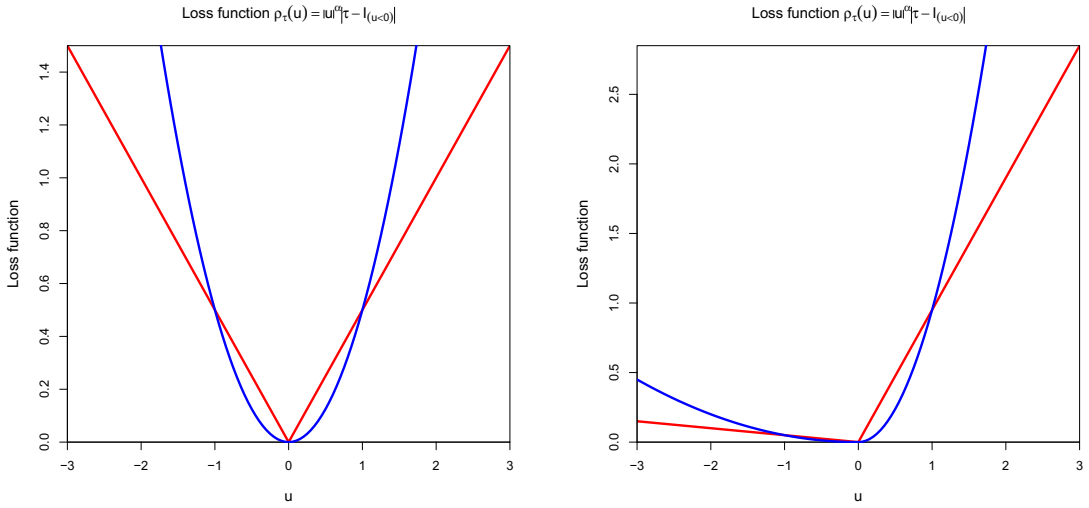

Figure 3: Loss function of expectiles (blue) where $\alpha = 2$ and quantiles (red) where $\alpha = 1$ for $\tau = 0.50$ (left) and $\tau = 0.95$ (right).

LQRcheck

In the unconditional case θ refers to the observation y that marks the τ-quantile. For the conditional τ-quantile, the minimizing θ depends on one or more covariates. The set represented by Θ is assumed to be defined such that the expectation is well defined. The concept of conditional quantile regression is introduced by (Koenker & Bassett 1978), who show that the solution $\widehat{\theta}$ of equation (5) yields a consistent estimator of the τ-quantile. A comprehensive survey on theory and applications of quantile regression is provided by Koenker (2005). The solution to the minimization problem given in equation (5) can be obtained numerically by linear programming (Koenker 2005). An alternative to the aforementioned loss function is proposed by Aigner et al. (1976) and Newey & Powell (1987). They suggest a quadratic loss function that leads to the estimation of so called expectiles. Contrary to quantiles, the loss function for expectiles is smooth. Examples are provided in figure (3). Quantiles and expectiles are called generalized quantiles. The optimization problem for a conditional generalized quantile is given by

$$l^\tau(X) = \arg\min_{f \in \mathcal{F}} \mathrm{E}\{\rho_\tau^\alpha(Y - f(X)\}, \alpha \in \{1, 2\} \tag{6}$$

with generalized loss function

$$\rho_\tau^\alpha(u) = |u|^\alpha \big|\tau - \mathbf{I}_{\{u<0\}}\big|. \tag{7}$$

Where $f(X)$ is a nonparametric function that depends on a one-dimensional covariate X and $\mathcal{F}$ describes the set, such that die expectation is well defined. The solution of equation (6) is called generalized quantile. The loss function in equation (7) leads to the estimation of quantiles for $\alpha = 1$ and expectiles for $\alpha = 2$. Expectiles are more efficient and faster to compute due to a differentiable loss function (Newey & Powell 1987). As for quantiles, the loss function for $\tau = 0.50$ is symmetric and the conditional expectile function in this case leads to the conditional expectation $\mathrm{E}(Y|X)$. However, the interest of this thesis is to characterize the tails and the center of the distribution of VWAPs. Both statistical parameters, quantiles and expectiles are well suited to perform this task. Even though there are differences between these two concepts, they are closely related. Jones (1994) demonstrates that expectiles are indeed quantiles of a distribution function G that is uniquely related to the CDF F. Similar findings are reported by Yao & Tong (1996) and Rossi & Harvey (2009). A comparison between both concepts concludes that one can numerically compute the quantile function from a set of expectiles (Waltrup et al. 2015). The interpretation of a quantile is straightforward as it represents the share τ of the observations below a certain threshold. Expectiles take the distance to the observation into account. Equation (6) with $\alpha = 2$ minimizes the overall distance to the expectile. Observations below the expectile cover $\tau \cdot 100\%$ of the overall minimized distance between observations and the respective expectile. Because of the fact that expectiles do not provide such an intuitive interpretation, in literature the focus is put more on conditional quantiles as stated by Waltrup et al. (2015).

3.3 Functional data models

This section extends the concept of generalized quantiles in the context of FDA and introduces the models that are used for dimension reduction. In general, a functional variable is is a map $Y : \Omega \to \mathcal{C}$, where Ω is the sample space and $\mathcal{C}$ the set of continuous functions on $\mathcal{T}$ (see e.g., Ferraty & Vieu (2006)). For the analysis in this thesis $\mathcal{T}$ corresponds to one day. By definition functional data is continuous, but in reality data is observed at discrete points. Denote $\mathbf{Y} = (Y_{tj}) \in \mathbb{R}^{T \times J}$. Where J is the number of curves, hence the number of days in the context of this thesis and T is the number of observations for one curve, hence the hours. The functional observation j is denoted by $Y_j(t)$. Denote further $\mathbf{B} = (B_{tl}) \in \mathbb{R}^{T \times p}$ as basis functions evaluated at the timings of measurement t. The basis functions evaluated at a certain t are donated by the corresponding row vector $\mathbf{B}_{t*} \in \mathbb{R}^p$. The timings of measurement are identical for all observations j. Thus the functional model for day j is given by

$$Y_j(t) = l_j^\tau(t) + u_j^\tau(t), \tag{8}$$

where $u_j^\tau(t)$ is an error term. The functional conditional generalized quantile curve can be approximated with basis functions by

$$l_j^\tau(t) = \delta^\top \mathbf{B}_{t*}, \tag{9}$$

where $\delta \in \mathbb{R}^p$ is a coefficient vector. The remainder of this subsection is dedicated to the applied models.

3.3.1 FPCA model

In case of the FPCA model, expectiles are estimated for each day individually. A separate estimation of the generalized quantile curves may lead to crossing quantiles/expectiles. In theory, this is not possible, but that phenomenon is well known to practitioners. The problem of crossing quantiles is addressed by Chernozhukov et al. (2010) with a natural monotonization approach, Dette & Volgushev (2008) for example use non-parametric techniques and Schnabel & Eilers (2013) propose estimation with a so called quantile sheet. The concept of sheet estimation for expectiles is introduced by Schnabel (2011). The underlying idea is to construct a surface from a set of non-crossing expectile curves. Therefore, a two-dimensional domain is spanned by the independent covariate t (the hours) and the asymmetry parameter τ as input variables. The expectile sheet estimates this surface directly by joint estimation of the expectile curves and can be constructed as a sum of tensor products of B-spline basis functions:

$$e(t, \tau) = \sum_{i=1}^{I} \sum_{j=1}^{J} a_{ij} B_i(t) \widetilde{B}_j(\tau). \tag{10}$$

The matrix $\mathbf{A} = [a_{ij}]$ is a coefficient matrix, $B_i(t)$ and $\widetilde{B}_j(\tau)$ are B-spline basis functions on the domains of t and τ. Eilers & Marx (1996) propose to use a huge quantity of knots and apply penalties on the coefficients of adjacent B-splines for smoothing. These penalized B-splines are also referred to as P-splines. For the estimation of the expectile sheets the least asymmetrically weighted squares (LAWS) algorithm introduced by Newey & Powell (1987) is applied. The expectile curve $e_j^\tau(t)$ for a certain τ of interest is obtained by evaluating the expectile sheet $e_j(t, \tau)$ for the respective τ. An implementation of expectile estimation in `R`

is available with the package `expectreg` by Sobotka et al. (2014), which is applied for the empirical analysis in this thesis.

The remainder of this subsection is dedicated to the application of FPCA to the expectile curves $e_j^\tau(t)$. For a review of FPCA and applications in explanatory analysis, modeling, forecasting and classification of functional data refer to Shang (2014). For the ease of notation, the asymmetry parameter τ is suppressed for the remainder of this subsection and $e_j^\tau(t)$ is denoted by $e_j(t)$. A crucial property in time series analysis is stationarity. A stochastic process is considered to be weakly stationary if its first and second moment are invariant with respect to time (see e.g., Lütkepohl (2005)). For the case of a functional time series this means that $e_j(t)$ has a common mean function $\mu(t) = \mathrm{E}\{e(t)\}$ and a common covariance function $K(s,t) = \mathrm{Cov}\{e(s), e(t)\}$ with $s, t \in \mathcal{T}$. Since a functional observation is in general of infinite dimension, a common tool for dimension reduction is FPCA. As in principal component analysis (PCA) for discrete data, orthogonal factors are obtained that describe the directions of the largest variation in the data as a linear combination (see e.g., Härdle & Simar (2015)). In the context of functional data, the factors are called principal component functions. If the covariance function of the expectile function $e(t)$ is continuous and square-integrable, i.e., $\iint_{\mathcal{T}} K^2(s,t)\,\mathrm{d}s\mathrm{d}t < \infty$, then $K(s,t)$ determines the kernel operator $\mathcal{K} : \phi \mapsto \mathcal{K}\phi$. This operator is defined as $(\mathcal{K}\phi)(s) = \int_{\mathcal{T}} K(s,t)\phi(t)\,\mathrm{d}t$ and the covariance function can be decomposed into

$$K(s,t) = \sum_{k=1}^{\infty} \lambda_k \phi_k(s)\phi_k(t). \tag{11}$$

With the eigenvalues λ_k for $k = 1, 2, \ldots$ of the operator $\mathcal{K}$ and their corresponding eigenfunctions ϕ_k. Eigenfunctions are also called principal component or basis functions and are orthogonal. By the Karhuhen-Loève (KH) transformation one can represent the stochastic process $\{e(t)\}_{t\in\mathcal{T}}$ as a linear combination of infinite orthogonal basis functions ϕ_k from $K(s,t)$. The KH transformation requires $\{e(t)\}_{t\in\mathcal{T}}$ to be a centered mean-square continuous process. A stochastic process is said to be centered if its expectation is zero. In general a process is not centered but can be centered by $\{e(t) - \mu(t)\}$, which has expectation zero for all $t \in \mathcal{T}$. A stochastic process is mean-square continuous if $\lim_{\varepsilon\to 0} \mathrm{E}[\{e(t+\varepsilon) - e(t)\}^2] = 0$. The KH transformation of a realization from the functional time series has the representation

$$e_j(t) - \mu(t) = \sum_{k=1}^{\infty} \alpha_{j,k}\phi_k(t) \tag{12}$$

with principal component scores

$$\alpha_{j,k} = \int_{\mathcal{T}} \{e_j(t) - \mu(t)\}\phi_k(t)\,\mathrm{d}t = \langle \{e_j(t) - \mu(t)\}, \phi_k \rangle \tag{13}$$

where $\langle \cdot, \cdot \rangle$ denotes the inner product. The scores $\alpha_{j,k}$ are uncorrelated across k, that means $\mathrm{E}(\alpha_{j,k}, \alpha_{j,l}) = 0$ for $k \neq l$, with $\mathrm{E}(\alpha_{j,k}) = 0$. The non-negative and non-increasing eigenvalues λ_k represent the variance of the the scores, formally $\mathrm{V}(\alpha_{j,k}) = \lambda_k$. The eigenvalues explain the variation in the data with non-increasing share. The truncated KH transformation with the first m principal components can be used to approximate the the expectile curves $e_j(t)$ by:

$$e_j(t) - \mu(t) \approx \sum_{k=1}^{m} \alpha_{j,k} \phi_k(t). \tag{14}$$

The truncated KH transformation reduces the dimension from infinity to m. Being aware of the theoretical framework about FPCA, in practice one has to estimate the empirical counterparts to the mean and covariance functions $\mu(t)$ and $K(s,t)$, as well as the eigenfunctions $\phi(t)$, the eigenvalues (λ_k) and the principal component scores $\alpha_{i,k}$. The empirical mean and covariance function are obtained as follows:

$$\widehat{\mu}(t) = \frac{1}{J} \sum_{j=1}^{J} e_j(t) \tag{15}$$

$$\widehat{K}(s,t) = \frac{1}{J} \sum_{j=1}^{J} \{e_j(s) - \widehat{\mu}(s)\}\{e_j(t) - \widehat{\mu}(t)\}. \tag{16}$$

The empirical kernel operator is estimated by

$$(\widehat{\mathcal{K}}\phi)(s) = \int_{\mathcal{T}} K(s,t)\phi(t)\,\mathrm{d}t. \tag{17}$$

The eigenfunctions $\widehat{\phi}_k t$ are computed from the estimated kernel operator and the scores are calculated as given in equation (13). An implementation for FPCA in `R` is available with the `fda` package by Ramsay et al. (2014), which is used for the empirical analysisin this thesis. There exists no unique rule to determine the number of scores m. In this thesis, m is selected that at least 95% of variation in the data is explained. As mentioned above, the data has two time dimensions. The intradaily dimension is reduced to m. Hence, the estimated score vector for day j and a certain τ is given by $\widehat{\alpha}_j(\tau) \in \mathbb{R}^m$. The interdaily time dynamics of the scores can be analyzed with a VAR model. This approach is explained in more detail in subsection (3.4).

3.3.2 FASTEC model

This subsection is dedicated to dimension reduction in the framework of a multivariate quantile regression (MQR) in a functional data context. The idea is to estimate the individual

curve variation jointly for a certain τ and avoid over-parametrization by reduced rank regression. Reduced rank regression is introduced by Izenman (1975). The idea is that in a multivariate regression setting the coefficient matrix does not need to have full rank, this means that one imposes linear restrictions on the regression coefficients. For an overview on theory and applications about multivariate reduced rank regression see Reinsel & Velu (1998). This subsection gives a brief description of the nonparametric curve model for quantile curves as introduced by Chao et al. (2015). This approach assumes a low-rank structure and does not impose distributional assumptions and the MQR for functional data $\mathbf{Y}$ is given by

$$\mathbf{q}^{\tau}(t) = \mathbf{B}\mathbf{\Gamma}, \tag{18}$$

where $\mathbf{q}^{\tau}(t) = (q_1^{\tau}(t), \ldots, q_J^{\tau}(t))$ and $\mathbf{B}$ are basis functions evaluated at timings of measurement. The number of basis functions is p and $\mathbf{\Gamma} \in \mathbb{R}^{p \times J}$ is a coefficient matrix. For the ease of notation, the asymmetry parameter τ is suppressed for the remainder of this subsection and the conditional quantile curve $q_j^{\tau}(t)$ is denoted by $q_j(t)$. If an estimator for $\mathbf{\Gamma}$ is available, Chao et al. (2015) suggest to apply SVD in order to obtain factors and factor loadings. The SVD is given by:

$$\mathbf{\Gamma} = \mathbf{U}\mathbf{D}\mathbf{V}^{\top}, \tag{19}$$

with rectangular diagonal matrix $\mathbf{D} \in \mathbb{R}^{p \times J}$ and unitary matrices $\mathbf{U} \in \mathbb{R}^{p \times p}$ and $\mathbf{V} \in \mathbb{R}^{J \times J}$. The diagonal elements in $\mathbf{D}$ represent the non-increasing singular values σ_k with $k = 1, \ldots, \min(p, J)$ of $\mathbf{\Gamma}$, which are the square roots of the eigenvalues of $\mathbf{\Gamma}$. Since $\mathbf{D}$ is rectangular, the number of singular values is $\min(p, J)$. The columns of the unitary matrix $\mathbf{U}$ contain the eigenvectors of $\mathbf{\Gamma}\mathbf{\Gamma}^{\top}$ and columns of $\mathbf{V}$ are the eigenvectors of $\mathbf{\Gamma}^{\top}\mathbf{\Gamma}$. The loading vector $\psi_j = (\psi_{j,1}, \ldots, \psi_{j,J})^{\top} \in \mathbb{R}^J$ for observation j is given by the jth row vector $\mathbf{V}_{j*}$ of $\mathbf{V}$. The kth factor curve is given by $f_k(t) = \mathbf{U}_{*k}^{\top}\mathbf{B}_{t*}\sigma_k$, where $\mathbf{U}_{*k} \in \mathbb{R}^p$ is the kth column vector of $\mathbf{U}$. If $\mathbf{\Gamma} = \mathbf{U}\mathbf{D}\mathbf{V}^{\top}$ than the quantile curve for observation j can be factorized by

$$q_j(t) = \sum_{k=1}^{r} \psi_{j,k} f_k(t), \tag{20}$$

where r is the number of non-zero singular values σ_k, i.e., the rank of $\mathbf{\Gamma}$. Only the first r entries of ψ_j are used in the factorized model (20). Substituting $f_k(t) = \mathbf{U}_{*k}^{\top}\mathbf{B}_{t*}\sigma_k$ into equation (20) gives

$$q_j(t) = \mathbf{\Gamma}_{*j}^{\top}\mathbf{B}_{t*} \tag{21}$$

where $\mathbf{\Gamma}_{*j} = (\sum_{k=1}^{r} \psi_{j,k}\sigma_k U_{1,k}, \ldots, \sum_{k=1}^{r} \psi_{j,k}\sigma_k U_{p,k})^\top$ denotes the jth column of the coefficient matrix $\mathbf{\Gamma}$ in model (18). An estimator for $\mathbf{\Gamma}$ is obtained as solution to the minimization of the loss function

$$\widehat{\mathbf{\Gamma}} = \arg\min_{\mathbf{\Gamma}\in\mathbb{R}^{p\times J}} \left\{ (TJ)^{-1} \sum_{t=1}^{T}\sum_{j=1}^{J} \rho_\tau^1(Y_{tj} - \mathbf{B}_{t*}^\top \mathbf{\Gamma}_{*j}) + \lambda\|\mathbf{\Gamma}\|_* \right\}, \tag{22}$$

where $\mathbf{Y} = (Y_{tj}) \in \mathbb{R}^{T\times J}$. The loss function in equation (22) can be split into two parts:

$$G(\mathbf{\Gamma}) = (TJ)^{-1} \sum_{t=1}^{T}\sum_{j=1}^{J} \rho_\tau^1(Y_{tj} - \mathbf{B}_{t*}^\top \mathbf{\Gamma}_{*j}) \tag{23}$$

$$H(\mathbf{\Gamma}) = \lambda\|\mathbf{\Gamma}\|_*. \tag{24}$$

Equation (23) represents the asymmetric loss function given in equation (7) and corresponds to the model fit. The second term of equation (22) denoted by $H(\mathbf{\Gamma})$ in equation (24) is for regularization. With tuning parameter λ and $\|\mathbf{\Gamma}\|_*$ being the nuclear norm of the coefficient matrix, defined as $\sum_{k=1}^{\min(p,J)} \sigma_k$. The nuclear norm regularization by Chao et al. (2015) is motivated by Yuan et al. (2007), who propose multivariate mean regression with a nuclear norm penalty. For the estimation of $\mathbf{\Gamma}$, Chao et al. (2015) apply the fast iterative shrinkage-thresholding algorithm (FISTA) proposed by Beck & Teboulle (2009). The algorithm is well suited to deal with optimization problems that include regularization and are of the form:

$$\min_{\mathbf{\Gamma}} \big\{ g(\mathbf{\Gamma}) + h(\mathbf{\Gamma}) \big\}, \tag{25}$$

where $g(\cdot)$ is a smooth and convex function with Lipschitz continuous gradient ∇g and $h(\cdot)$ is continuous convex. Since $G(\mathbf{\Gamma})$ is non-smooth the smoothing proposed by Nesterov (2005) is applied. As a first step, dual variables Θ_{tj} are introduced for each pair tj with

$$\Theta_{tj} = \begin{cases} \tau, & \text{if } Y_{tj} > \mathbf{B}_{t*}^\top \mathbf{\Gamma}_{*j} \\ \tau - 1, & \text{if } Y_{tj} \leq \mathbf{B}_{t*}^\top \mathbf{\Gamma}_{*j}. \end{cases} \tag{26}$$

In a second step $G(\mathbf{\Gamma})$ is rewritten as the maximization problem

$$G(\mathbf{\Gamma}) = \max_{\Theta_{tj}\in[\tau-1,\tau]} (TJ)^{-1} \sum_{t=1}^{T}\sum_{j=1}^{J} \Theta_{tj}(Y_{tj} - \mathbf{B}_{t*}^\top \mathbf{\Gamma}_{*j}). \tag{27}$$

The support of Θ_{tj} is the interval $[\tau-1, \tau]$ in order to fulfill the convex set conditions given by Nesterov (2005). Denote $\mathbf{\Theta} = (\Theta_{tj}) \in \mathbb{R}^{T\times J}$ and introduce a regularization parameter $\kappa > 0$, then a smooth approximation to $G(\mathbf{\Gamma})$ is obtained via

$$G_\kappa(\mathbf{\Gamma}) = \max_{\Theta_{tj}\in[\tau-1,\tau]} \left\{ (TJ)^{-1} \sum_{t=1}^{T}\sum_{j=1}^{J} \Theta_{tj}(Y_{tj} - \mathbf{B}_{t*}^\top \mathbf{\Gamma}_{*j}) - \frac{\kappa}{2}\|\mathbf{\Theta}\|_F^2 \right\}. \tag{28}$$

Where $\|\mathbf{A}\|_F = \sqrt{\sum_{i=1}^{n}\sum_{j=1}^{m}|A_{ij}|^2}$ is the Frobenius norm of matrix $\mathbf{A} = (A_{ij}) \in \mathbb{R}^{n\times m}$. That the approximation in equation (28) gets closer to $G(\mathbf{\Gamma})$ in equation (23) as $\kappa \to 0$. The penalization term $\frac{\kappa}{2}\|\mathbf{\Theta}\|_F^2$ is strongly convex and therefore the optimal solution $\mathbf{\Theta}^*(\mathbf{\Gamma}) = [[(\kappa TJ)^{-1}(\mathbf{Y} - \mathbf{B\Gamma})]]_\tau$ is unique for each $\mathbf{\Gamma}$. The matrix notation $[[\mathbf{A}]]_\tau = [[A_{ij}]]_\tau$ is a function defined as

$$[[A_{ij}]]_\tau = \begin{cases} \tau, & \text{if } A_{ij} \geq \tau \\ A_{ij}, & \text{if } \tau - 1 < A_{ij} < \tau \\ \tau - 1, & \text{if } A_{ij} \leq \tau - 1 \end{cases} \tag{29}$$

and projects every component A_{ij} to the interval $[\tau - 1, \tau]$. The smooth $G_\kappa(\mathbf{\Gamma})$ is for $\kappa > 0$ well defined, convex, continuously-differentiable in $\mathbf{\Gamma}$ and has Lipschitz gradient

$$\nabla G_{\tau,\kappa}(\mathbf{\Gamma}) = -(TJ)^{-1}\mathbf{B}^\top[[(\kappa TJ)^{-1}(\mathbf{Y} - \mathbf{B\Gamma})]]_\tau. \tag{30}$$

The Lipschitz constant is given by $M = (\kappa J^2T^2)^{-1}\|\mathbf{B}\|^2$ and $\kappa = \frac{\epsilon}{2TJ}$, where ϵ denotes a certain accuracy level. For more details on the smoothing, theoretical derivations and convergence analysis see section (2) in Chao et al. (2015). The smooth approximation $G_\kappa(\mathbf{\Gamma})$ fulfills the conditions for $g(\cdot)$ in equation (25) and the FISTA of Beck & Teboulle (2009) can be applied to the optimization problem

$$\min_{\mathbf{\Gamma}} \big\{G_\kappa(\mathbf{\Gamma}) + H(\mathbf{\Gamma})\big\}. \tag{31}$$

As a last step the proximity operator $S_\lambda(\cdot)$ of $\lambda\|\cdot\|_*$ is introduced

$$S_\lambda(\mathbf{\Gamma}) = \mathbf{U}(\mathbf{D} - \lambda\mathbf{I}_{p\times J}) + \mathbf{V}^\top, \tag{32}$$

where the SVD of $\mathbf{\Gamma} = \mathbf{UDV}^\top$ and the $(p \times J)$ rectangular identity matrix $\mathbf{I}_{p\times J}$ has diagonal elements equal to one. For more details about the proximity operator in the context of FASTEC refer to Chao et al. (2016). The smoothing FISTA summarizes the optimization problem for the multivariate quantile regression in algorithm (1).

Derivation of the penalizing parameters λ and κ are provided by Chao et al. (2015). However, they use for simulation and application $\kappa = 0.0001$, inspired by Chen et al. (2012). Furthermore, Chao et al. (2015) select λ by the "pivotal principle" which adapts better to the data. Therefore they define a random variable $\Lambda = (TJ)^{-1}\|\mathbf{B}^\top\mathbf{W}\|$ with $\mathbf{W} = (W_{tj}) \in \mathbb{R}^{T\times J}$ and $W_{tj} = \mathbf{I}_{(U_{tj}\leq 0)} - \tau$, where $\{U_{tj}\}$ are i.i.d. uniform (0,1) random variables. Hence, Λ does not depend on the coefficient matrix $\mathbf{\Gamma}$, but on the design of the covariate matrix $\mathbf{B}$. The

Algorithm 1: Smoothing fast iterative shrinkage-thresholding algorithm (SFISTA)

Data: $\mathbf{Y}$, $\mathbf{B}$, λ, κ, M, $\tau \in (0,1)$

Result: $\widehat{\mathbf{\Gamma}}_\tau = \mathbf{\Gamma}_{\tau,H}$

Initialization: $\mathbf{\Gamma}_{\tau,0}$, $\mathbf{\Omega}_{\tau,1} = 0$, step size $\delta_1 = 1$;

for $h = 1, 2, \ldots, H$ **do**

$\mathbf{\Gamma}_{\tau,h} = S_{\lambda/M}\Big(\mathbf{\Omega}_{\tau,h} - \frac{1}{M}\nabla \mathbf{G}_{\tau,\kappa}(\mathbf{\Omega}_{\tau,h})\Big)$;

$\delta_{h+1} = \frac{1+\sqrt{1+4\delta_h^2}}{2}$;

$\mathbf{\Omega}_{\tau,h+1} = \mathbf{\Gamma}_{\tau,h} + \frac{\delta_h - 1}{\delta_{h+1}}(\mathbf{\Gamma}_{\tau,h} - \mathbf{\Gamma}_{\tau,h-1})$;

end

tuning parameter is then obtained via

$$\lambda = 2 \cdot \Lambda(1-\alpha|\mathbf{B}), \tag{33}$$

where the $(1-\alpha)$-quantile of Λ conditional on $\mathbf{B}$ is denoted by $\Lambda(1-\alpha|\mathbf{B})$. The "pivotal principle" is proposed by Belloni & Chernozhukov (2011) for high-dimensional quantile regression. They further set $\alpha = 0.1$, which is also implemented by Chao et al. (2015).

From the estimated coefficient matrix $\widehat{\mathbf{\Gamma}}_\tau$ the vectors of factor loadings $\widehat{\psi}_j(\tau) \in \mathbb{R}^r$ are obtained. These loading vectors contain the first r entries that correspond to the non-zero singular values of $\widehat{\mathbf{\Gamma}}_\tau$. Hence, intradaily time dimension of a quantile curve $q^\tau(t)$ reduces to r. In order to analyze the interdaily time dynamics, a VAR model is applied to the vector of estimated factor loadings $\widehat{\psi}_j(\tau)$. This approach is explained in the next subsection.

3.4 Forecasting generalized quantiles

This subsection describes how the interdaily time dynamics of the generalized quantiles are analyzed and used for forecasts. Both models introduced above capture the variation during day j through the estimated vector of scores $\widehat{\alpha}_j(\tau)$ or factor loadings $\widehat{\psi}_j(\tau)$. Aue et al. (2015) use a functional auto regressive model to analyze and forecast FPCA scores. Cabrera & Schulz (in press) apply a VAR model with exogenous variables (VARX) to model and forecast the time dynamics of functional principal component (FPC) scores. Following their approach, the time dynamics of the FPC scores $\widehat{\alpha}_j(\tau)$ and factor loadings $\widehat{\psi}_j(\tau)$ are modeled with the VARX model

$$\mathbf{z}_j = \sum_{w=1}^{s} \mathbf{\Phi}_w \mathbf{z}_{j-w} + \mathbf{\Pi}\mathbf{x}_j + \eta_j, \tag{34}$$

where $\mathbf{z}_j$ is the vector of estimated FPC scores or factor loadings for day j. The coefficient matrix for lag w is given by $\mathbf{\Phi}_w$, $\mathbf{x}_j$ are the exogenous variables with coefficient matrix $\mathbf{\Pi}$ and η_j represents a white noise process. For more details on multivariate time series modeling refer to Lütkepohl (2005). Forecasts from the VARX model for h steps ahead are obtained by

$$\widehat{\mathbf{z}}_{j+h} = \sum_{w=1}^{s} \widehat{\mathbf{\Phi}}_w \mathbf{z}_{j+h-w} + \widehat{\mathbf{\Pi}} \mathbf{x}_{j+h}. \tag{35}$$

The forecast $\widehat{\mathbf{z}}_{j+h}$ is the forecasted vector either of FPC scores, denoted as $\widetilde{\widehat{\alpha}}_{j+h}(\tau)$ or factor loadings $\widetilde{\widehat{\psi}}_{j+h}(\tau)$. From these vectors the computation of the generalized quantile function for the h-step ahead forecast is straightforward. Denote $\widehat{e^{\tau}}_{j+h}(t)$ the h-step ahead forecast for the expectile curve for a certain τ, then the forecast with the FPCA model is given by

$$\widehat{e^{\tau}}_{j+h}(t) = \widehat{\mu}^{\tau}(t) + \sum_{k=1}^{m} \widetilde{\widehat{\alpha}}_{j+h,k}(\tau) \widehat{\phi}_k^{\tau}(t). \tag{36}$$

Denote further the h-step ahead forecast for the quantile function by $\widehat{q^{\tau}}_{j+h}(t)$ and the forecast based on the FASTEC model is

$$\widehat{q^{\tau}}_{j+h}(t) = \sum_{k=1}^{r} \widetilde{\widehat{\psi}}_{j+h,k}(\tau) \widehat{f}_k^{\tau}(t). \tag{37}$$

Forecasts for the generalized quantiles $\widehat{l}^{\tau}_{j+h}(t)$ from equation (36) and (37) correspond to the deseasonalized component. Hence, a forecast for the seasonal component $\widehat{\Lambda}_{t,j+h}$ obtained by equation (2) needs to be added. Consequently the h-step ahead forecast for the generalized quantile curve for the VWAP is given by:

$$\widetilde{\widehat{l}}^{\tau}_{j+h}(t) = \widehat{l}^{\tau}_{j+h}(t) + \widehat{\Lambda}_{t,j+h}. \tag{38}$$

4 Results

This section shows the application of the above presented models to the VWAP series and the results. The data is split into train data for the period (2014-01-01 to 2015-12-31) and test data for the period (2016-01-01 to 2016-12-31). First, an evaluation for the in-sample period is presented. Second, a rolling window out-of-sample approach is used to evaluate the model performance in a real world setting. Aggarwal et al. (2009) stress the necessity of longer test periods which is supported by Weron (2014) who points out that *"[...] carefully selected one-week periods, [...] generally ignore the problem of special days (holidays, near-holidays)"* and he suggest to consider test periods of more months. For the probabilistic analysis expectile curves (FPCA model) and quantile curves (FASTEC model) are computed for $\tau = 1\%, 5\%, 25\%, 50\%, 75\%, 95\%$ and 99%. The same levels are used in Cabrera & Schulz (in press) in order to forecast distributional characteristics of load consumption. The pair of forecasted generalized quantile curves $\left(\widetilde{\widetilde{l}}_j^{\tau}(t), \widetilde{\widetilde{l}}_j^{1-\tau}(t)\right)$ for $\tau \in (0, 0.50)$ allows to construct the $(1-2\tau)\cdot 100\%$ forecast interval, denoted by:

$$\widehat{\pi}_j^{1-2\tau}(t) = [\widetilde{\widetilde{l}}_j^{\tau}(t), \widetilde{\widetilde{l}}_j^{1-\tau}(t)]. \tag{39}$$

The performance of the forecasted intervals is measured to which share it covers observed VWAPs. Define for $\tau \in (0, 0.50)$ the forecast interval coverage (FIC) by

$$\text{FIC}(1-2\tau) = \frac{1}{24\cdot J}\sum_{t=1}^{24}\sum_{j=1}^{J}\mathbf{I}_{\{\widetilde{P}_{tj}\in\widehat{\pi}_j^{1-2\tau}(t)\}}\,. \tag{40}$$

Where $\widetilde{P}_{t,j}$ denotes the observed VWAP at day j and time of the day t. The indicator function $\mathbf{I}$ takes value one if the observed VWAP is within the forecasted interval. For the train data $J = 730$ and for the test data $J = 365$. In case the interest is in a point forecast for the VWAPs at the following day, only the expectile / quantile curves for $\tau = 0.50$ needs to be considered. While the 50% expectile corresponds to the conditional mean, the median is also suitable as a point forecast (Gneiting 2011). In order to compare the point forecasts, both are evaluated with RMSE and mean absolute error (MAE), defined as

$$\text{RMSE} = \sqrt{\frac{1}{24\cdot J}\sum_{t=1}^{24}\sum_{j=1}^{J}\left\{\widetilde{\widetilde{l}}_j^{0.50}(t) - \widetilde{P}_{tj}\right\}^2} \tag{41}$$

$$\text{MAE} = \frac{1}{24\cdot J}\sum_{t=1}^{24}\sum_{j=1}^{J}\left|\widetilde{\widetilde{l}}_j^{0.50}(t) - \widetilde{P}_{tj}\right|. \tag{42}$$

4.1 Train data

The dynamics of the VWAP series are first investigated within the train data. The VWAP series and the exogenous variables are first deseasonalized as described in section (3.1). The exogenous variables contain of 24 observations for each day. Using all of them in the VARX model would induce overparametrization. Such an issue arises often in multivariate regression settings and in general leads to prediction uncertainty. The variation of the exogenous time series can be utilized by decomposing the variance matrix with PCA and select PCs and corresponding scores that explain a considerable proportion of the variance. In order to apply PCA, the deseasonalized series are normalized and the number of PCs is selected that at least 95% of variation is explained. The explanatory power of the first seven PCs for the train period is given in table (3). The number of selected components varies for among the exogenous variables. While for DAspot seven PCs are chosen, for RLact and RLmk three components are sufficient. Six PCs are required for RLdiff to explain at least 95% of variation.

	Exogenous variable			
PC	$DAspot$	$RLact$	$RLmk$	$RLdiff$
1	0.659	0.790	0.801	0.677
2	0.127	0.102	0.110	0.115
3	0.081	0.064	0.059	0.086
4	0.035	0.016	0.012	0.033
5	0.024	0.012	0.008	0.025
6	0.014	0.004	0.003	0.015
7	0.012	0.003	0.002	0.009
Sum	0.952	0.991	0.996	0.959

Table 3: Proportion of explained variance of first seven PCs of the exogenous variables.


VWAP_FPCA_Training

4.1.1 FPCA model

The FPCA model requires first a joint estimation of expectile curves for each day and reduces in a second step the dimension of the nonparametric functions for a certain τ for all days. The expectile sheets are computed for the deseasonalized VWAP series with penalized spline smoothing. The penalty term is chosen with generalized cross validation in order to obtain optimal smoothing. Figure (4) presents estimated expectile sheets for 2014-01-20 and 2014-01-21. The stochastic price component shows on both days a similar shape and its

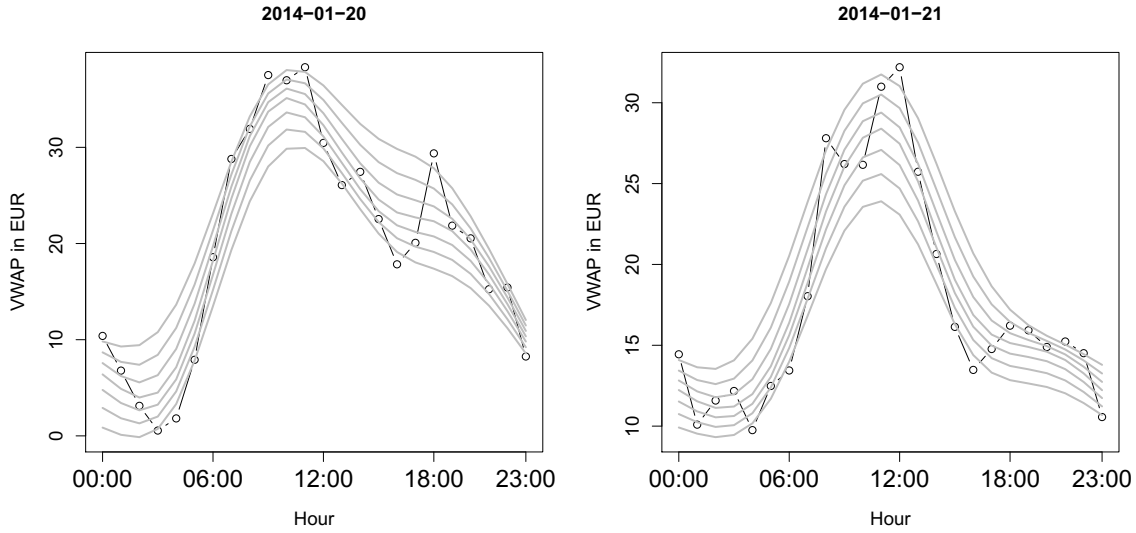

Figure 4: Stochastic component of VWAP series and corresponding estimated expectile curves for $\tau = 0.01, 0.05, 0.25, 0.50, 0.75, 0.95, 0.99$ (grey) in ascending order from bottom to top.

`VWAP_FPCA_Training`

dispersion can be described through the fitted expectile curves.

The obtained expectile curves need to be centered. Hence, for each asymmetry parameter τ, the empirical mean function $\widehat{\mu}^{\tau}$ is subtracted from the corresponding expectiles. The 50% expectile should have mean zero which is implied from the deseasonalization. But those below and above the center of the distribution are different from zero. Figure (5) shows the empirical mean functions for all τ-levels. As expected, the 50% expectile is roughly zero, the other τ-levels show peaks in the morning and evening hours. The peaks are more distinct, the closer τ gets to its boundaries, representing the tails of the distribution.

The number of FPCs is selected that at least 95% of variation for a certain τ level is explained. Table (4) gives information on the explanatory power of the first four FPCs. Those are sufficient to explain the desired variation of the functional time series for each τ level. By far the highest proportion provides the first FPC with about 70% for all τ.

The eigenfunctions $\widehat{\phi}_k^{\tau}$ of the FPCs and the time series of the corresponding scores $\widehat{\alpha}_{j,k}(\tau)$ are illustrated for $\tau = 0.50$ in figure (6) and figure (7). The first FPC describes the total variation in the level of the VWAP. Variation in the height of the price level during peak hours is reflected by FPC2. The third FPC gives information on how the location of the price level varies during the peak hours. FPC4 gives information on the slope of the price curve. However, the interpretation of the latter three components is not that straightforward. After all they do not explain too much of the variation in the data compared to FPC1. The shape

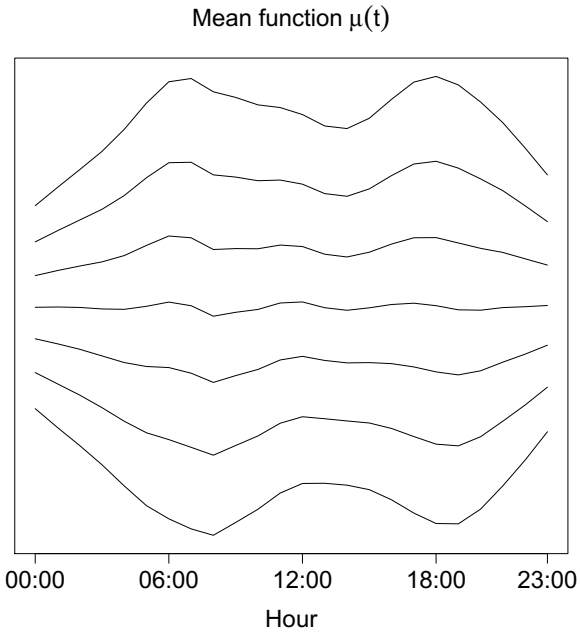

Figure 5: Estimated mean functions $\widehat{\mu}^{\tau}(t)$ for $\tau = 0.01, 0.05, 0.25, 0.50, 0.75, 0.95$ and 0.99 in ascending order from bottom to top.

VWAP_FPCA_Training

	Expectile level τ						
FPC	0.01	0.05	0.25	0.50	0.75	0.95	0.99
1	0.704	0.703	0.701	0.698	0.699	0.699	0.697
2	0.145	0.141	0.138	0.135	0.132	0.131	0.132
3	0.087	0.089	0.092	0.095	0.098	0.101	0.102
4	0.034	0.035	0.036	0.037	0.036	0.036	0.037
Sum	0.970	0.969	0.967	0.965	0.966	0.967	0.968

Table 4: Proportion of explained variance of the first four FPC for the VWAP series.

VWAP_FPCA_Training

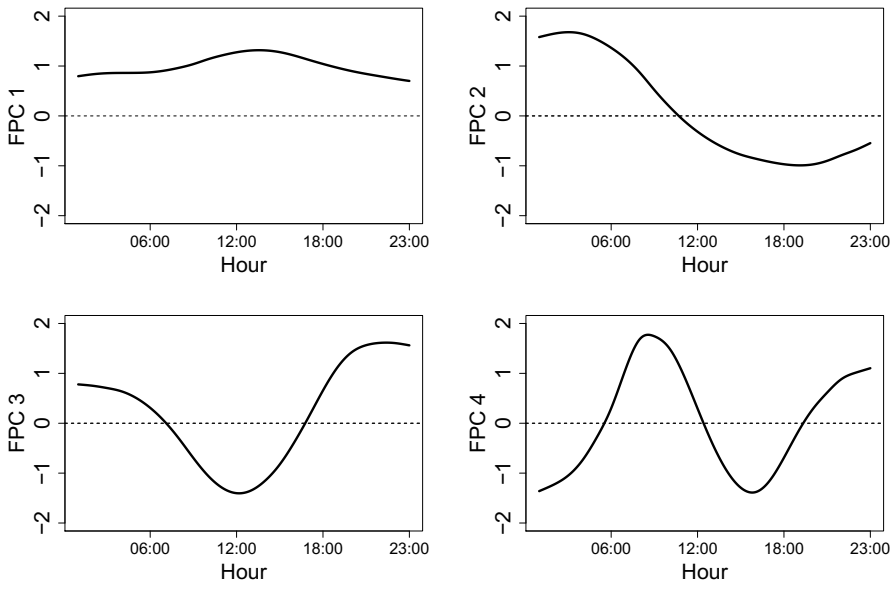

Figure 6: Eigenfunctions $\widehat{\phi}_k^{\tau}$, $(k = 1, \ldots, 4)$ of the first four FPCs for the 50% expectile curves.

VWAP_FPCA_Training

of the eigenfunctions of the first three FPC is quite similar to those Cabrera & Schulz (in press) present for total load. That seams plausible because total load and prices are linked to each other through the merit order curve. The scores give information about the underlying variable given the interpretation of the corresponding FPC. The interpretation of the first FPC corresponds to the variation in the level of VWAPs. A positive value on the respective score to FPC1 indicates that observed VWAP is above average VWAP. Consequently, a negative score on FPC1 is related to prices below average. As mentioned in section (3), the scores are analyzed with a VAR(X) model. Therefore they should be stationary. From a visual point of view, one can assume that the FPC score series are stationary. In order to validate this visual impression, the scores for all τ-expectile curves are tested with the Augmented-Dickey-Fuller (ADF) test and Kwiatkowski-Phillips-Schmidt-Shin (KPSS) test. The latter tests the null hypothesis of stationarity and ADF tests the null hypothesis of a unit root (see e.g., Greene (2007)). The tests are conducted with the `R` package `tseries` by Trapletti & Hornik (2016). While the KPSS test reports p-values higher than 10% for all score series, the ADF test reports p-values smaller than 1%. Stationarity is not rejected by KPSS and ADF rejects a unit root. Hence, stationarity can be assumed.

The time dynamics of the FPC scores are analyzed with a VAR(X) model. The models

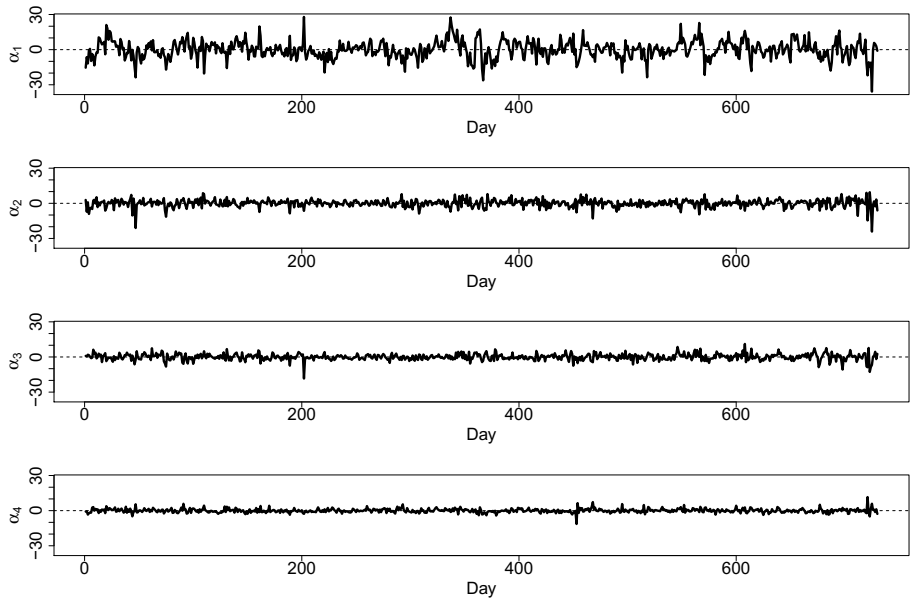

Figure 7: Time series of scores $\widehat{\alpha}_k(\tau)$, $(k = 1, \ldots, 4)$ of the first four FPCs for the 50% expectile curves.

VWAP_FPCA_Training

differ from each other regarding the included exogenous information. The fitted scores from the VAR(X) models are translated into expectile curves through KL transformation. As a last step, the seasonal component is added. The number of lags in the VAR(X) is selected with Akaike information criteria (AIC) and Bayesian information criteria (BIC). While AIC is more suited for model selection and to obtain explanatory power, the BIC is better suited for forecasting (see e.g., Shmueli (2010)). As stated in the beginning of this section, models are evaluated according to RMSE, MAE and FIC. Table (6) reports results on the estimation procedure based on BIC. The results with lag order selection by AIC is given in table (11) in the appendix. In order to distinguish between the models, for the remainder of this thesis each approach is named according to the estimation procedure. Hence, the approach where FPC scores are forecasted with RLmk as exogenous variable is denoted by FPCA RLmk. In case no exogenous variable is used, the model is named FPCA no. As a naive forecast serves the price from the day-ahead auction which is denoted by the variable name DAspot. The deterministic trend model is denoted by Trend. It turns out that the naive forecast provides a competitive RMSE of 6.709. The FPCA DAspot model exhibits the best in-sample fit among the VAR(X) models. Residual load provides also important information, but actual values would not be available in a real world setting. Interestingly, the price from the day-ahead

auction which is based on expected residual load contributes better to forecast accuracy in the train data than actual residual load data. Using RLmk as exogenous variable the model performance declines compared to FPCA DAspot and FPCA RLact. Almost no information gain is obtained by the model with RLdiff as exogenous variable compared to FPCA no. Since RLdiff shows almost no correlation with the VWAP series (see section (2.2)), this is not surprising. The Trend model performs worst among all point forecasts with a RMSE of 9.598. Hence, an application of the FPCA modeling technique adds valuable information compared to a simple trend model. The models selected with AIC slightly outperform those selected with BIC. The ranking of the models according their probabilistic performance is the same as for the point forecast. The forecasted intervals are not at all able to cover a proportion around $(1 - 2\pi) \cdot 100\%$ of observed VWAPs. The FIC(0.98) from the FPCA DAspot model is with 30% quite low and is even lower for the remaining models. Consequently, the more narrow the intervals become, the lower is the FIC. The proportion covered by the intervals of the inter expectile range FIC(0.50) is less than 10% for all FPCA models.

An example that illustrates forecasts by the FPCA DAspot, the Trend and DAspot model is illustrated in figure (8) for 2014-01-23 and 2014-01-24. The trend component provides the general daily pattern. On 2014-01-23, the estimated curve for $\tau = 0.50$ deviates strongly from the VWAP curve and the forecast interval $\widehat{\pi}^{0.98}$ does not at all provide a reasonable interval for VWAPs. However, the situation changes on 2014-01-24. Here the estimated expectiles for $\tau \neq 0.50$ expand a reasonable band around the point forecast that is able to capture the VWAP series to some extent.

4.1.2 FASTEC model

The application of the nonparametric MQR to the deseasonalized VWAP is presented in this section. Asymmetry parameters τ as described above. There are 24 timings of measurement corresponding to the 24 hours a day. The B-spline basis functions are evaluated on those time points with 4 degrees of freedom (df). Those are selected according to Chao et al. (2015) by $df = \lceil 24^{0.4} \rceil = 4$, where $\lceil \cdot \rceil$ means the next higher integer value. The tuning parameter λ is obtained for each τ considering the approach in equation (33) and can be found in table (10) in the appendix. The regularization parameter κ is set to 0.0001. The SVD of $\widehat{\mathbf{\Gamma}}$ provides the estimated factor curves and factor loadings. The number of non-zero singular values for each τ is four, that means the number of factors r is also four. The factor curves $\widehat{f}_k^{\tau}$ for the conditional median are displayed in figure (9). The daily factor curves differ substantial to

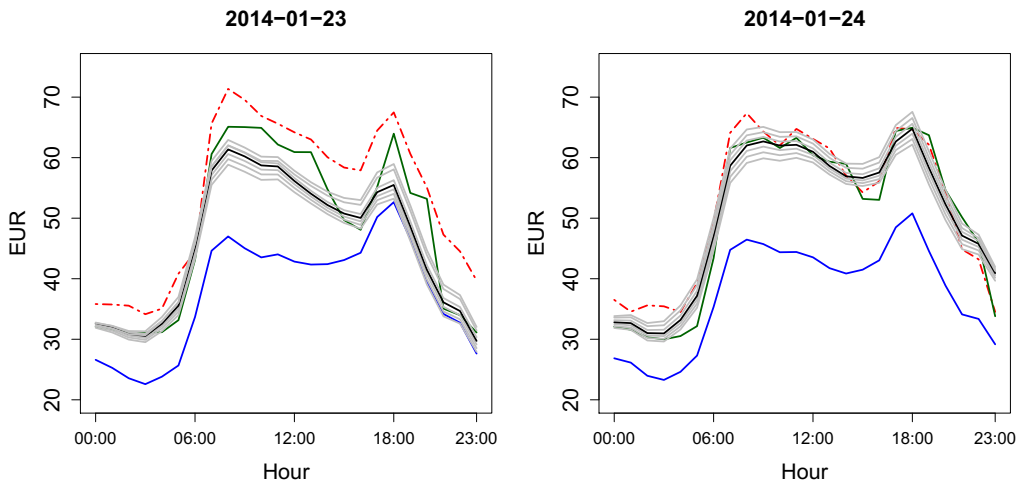

Figure 8: Actual VWAP curve (dashed red), curve estimates for 50% expectile and for $\tau = 0.01, 0.05, 0.25, 0.75, 0.95, 0.99$ (grey) from FPCA DAspot, DAspot (darkreen) and Trend model (blue).

VWAP_FPCA_Training

the eigenfunctions in the FPCA model. No meaningful interpretation of those curves can be found. The explanatory contribution of the factors is summarized for all τ in table (5). Since the number of factors is equal to df, the explanatory power of the four factors sum up to 100%. Most contribution stems from the first factor which explains for the different τ-levels about 99%. Hence, the remaining three factors contribute only a minor share.

	Quantile level τ						
Factor	0.01	0.05	0.25	0.50	0.75	0.95	0.99
1	0.9936347	0.9994612	0.9944273	0.9815879	0.9941608	0.9993751	0.9982057
2	0.0063395	0.0003949	0.0044391	0.0148493	0.0047429	0.0004605	0.0017644
3	0.0000235	0.0001330	0.0010649	0.0033379	0.0010248	0.0001523	0.0000274
4	0.0000023	0.0000109	0.0000687	0.0002250	0.0000715	0.0000122	0.0000025

Table 5: Proportion of explained variance of coefficient matrix by factors.

VWAP_FASTEC_Training

The time series of the factor loadings $\widehat{\psi}_{j,k}(\tau)$ are displayed in figure (10) for the coefficient matrix on the conditional median. As in the previous section, the factor loadings for all τ are tested for stationarity with the ADF test and the KPSS test. The test result is similar to the scores from the FPCA model. Stationarity can be assumed since the ADF rejects

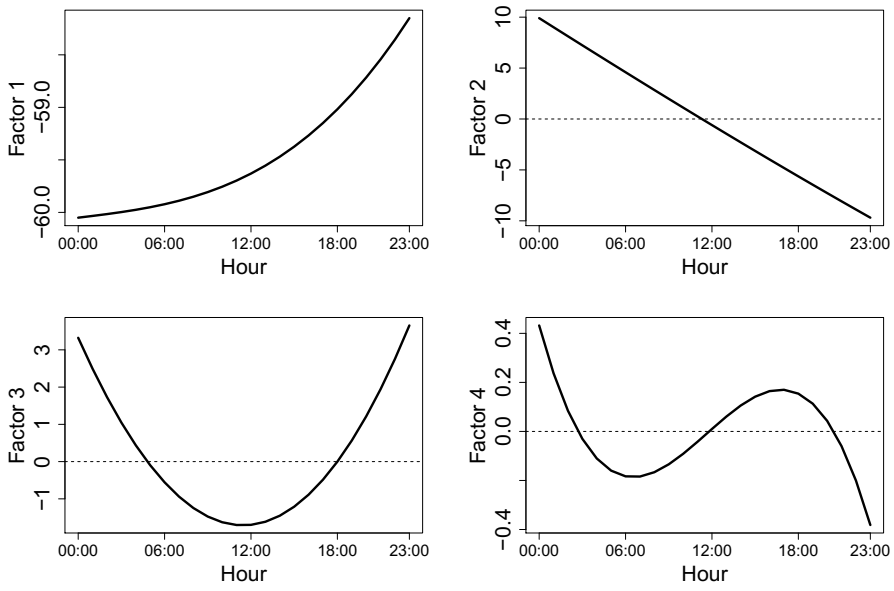

Figure 9: Factor curves $\widehat{f}_k^{\tau}$, $(k = 1, \ldots, 4)$ of the coefficient matrix for 50% quantile curves.

VWAP_FPCA_Training

the hypothesis of a random walk for each series with a p-value below 1%. The KPSS test further does not reject the hypothesis of stationarity at 10% in most cases. An exception are the loadings for the 3rd factor. Here the KPSS test rejects stationarity at a significance level of 5% for $\tau = 0.01$ and $\tau = 0.75$. The KPSS test rejects further stationarity at 10% significance for $\tau = 0.95$ and $\tau = 0.99$. However, stationarity can never be rejected with a significance level of 1%.

The fit from the MQR on the deseasonalized VWAP series is depicted in figure (11). Estimated quantile curves for asymmetry parameters $\tau \leq 0.50$ are pretty close to each other. Especially those for the conditional 25% and 50% quantile are overlapping for some hours. This is completely different for those above the conditional median which are much more far apart from each other. A reason for this could be that in general during peak hours prices are higher than during off peak and show further higher variation. In particular extreme negative prices may drag down the estimations for conditional quantiles below the median. The fit of the deseasonalized component from the MQR is quite distinct from the fit of the expectile curves displayed above in figure (4) which show the same time period.

In order to model the interdaily dependencies of the factor loadings, a VAR(X) model is applied. As above, the lag order of the endogenous variable is selected according to BIC and AIC. The model results after recomputing the daily curves form the factor loadings are

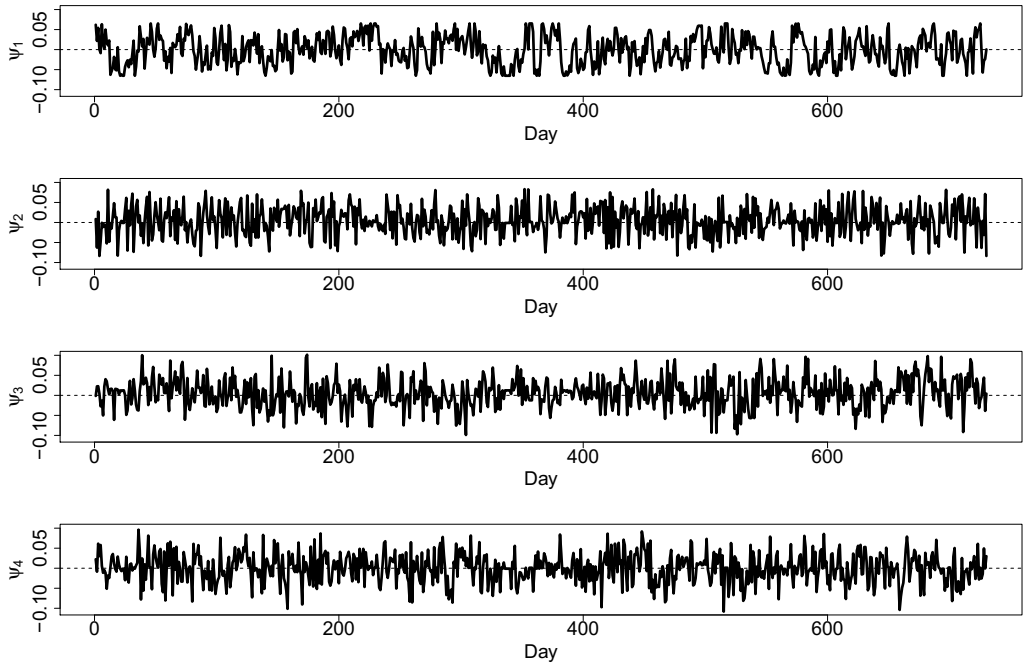

Figure 10: Time series of factor loadings $\widehat{\psi}_k(\tau)$, $(k = 1, \ldots, 4)$ of four factors for the 50% quantile curves.

VWAP_FASTEC_Training

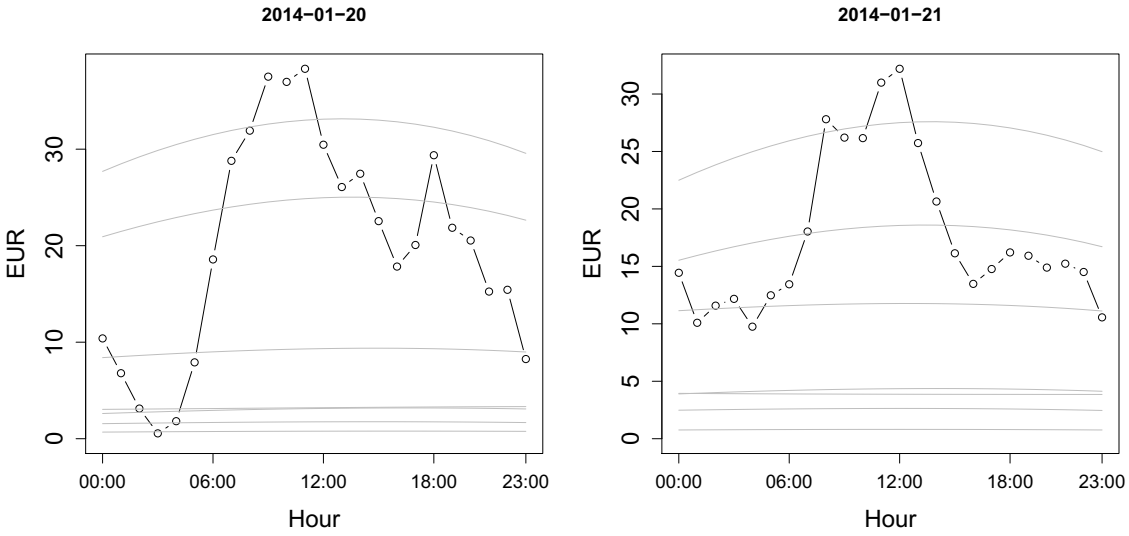

Figure 11: Stochastic component of VWAP series and corresponding estimated quantile functions for $\tau = 0.01, 0.05, 0.25, 0.50, 0.75, 0.95, 0.99$ (grey) in ascending order from bottom to top.

VWAP_FASTEC_Training

displayed in table (6) with VAR lag selection according to BIC and table (11) in the appendix where the lag order is selected by AIC. The RMSE among the FASTEC models is with about 8.508 lowest for FASTEC DAspot and increases to 8.991 for FASTEC no. Hence, the point forecasts from the FASTEC models contain lower accuracy than those from the FPCA models. Furthermore, the RMSE of the FASTEC models is less distinct among the different VAR(X) specification as the RMSE of the FPCA models. This indicates that exogenous information do not add that much additional information in case of the FASTEC approach. Nevertheless, the FASTEC models outperform the simple deterministic trend. Moreover, the FIC increases considerably compared to the FPCA models. The FIC(0.98) of the best performing VAR model reaches 76%. This is more than double of the reported FIC(0.98) in case of the FPCA DAspot model. The FIC(0.98) of the remaining FASTEC models is at least 68%. The same tendency is observed for the FIC(0.50) and FIC(0.90). For the latter FIC, the FASTEC models report almost a quadruple of those from the FPCA model. As above, models selected by AIC outperform those selected by BIC.

An exemplary illustration of the results is shown in figure (12). The graphs in the figure represent forecasts from the models FASTEC DAspot, Trend and DAspot for 2014-01-23 and 2014-01-24. One observes that the dispersion of the forecast intervals is much more wider than those illustrated for the FPCA model in figure (8). The forecast interval $\widehat{\pi}^{0.98}$ is able to capture the realized VWAP series quite reasonable on 2014-01-24 with a few exceptions in the morning peak hours. The contrary is the case on 2014-01-23, where during most hours even the estimated 99% quantile curve is below observed VWAPs.

4.2 Test data

This section reports the model performance for the year 2016. Out-of-sample forecasts are computed with a forecast horizon of one day. Forecasts regarding the deterministic trend and different generalized quantiles of the deseasonalized VWAP are computed using the models introduced in section (3). The forecasts are based on a rolling window approach. The length of the train period gives the length of the window. Hence, in each step, models are fitted on a two year period and are then used to construct forecasts for the seasonal and stochastic component for the following day. The results are summarized in table (7) for VAR(X) lag selection by BIC and for those selected with AIC in table (12) in the appendix. The out-of-sample performance a with shorter window can be found in table (14) for a 30 day rolling window and in table (13) for a 60 day rolling window in the appendix. For the out-of-sample

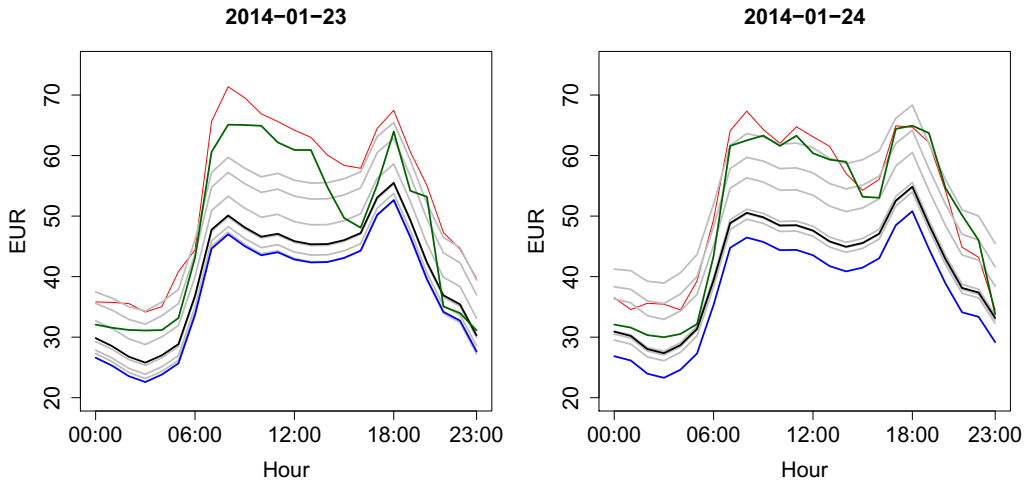

Figure 12: Actual VWAP curve (dashed red), curve estimates for 50% quantile and for $\tau = 0.01, 0.05, 0.25, 0.75, 0.95, 0.99$ (grey) from FASTEC DAspot, DAspot (darkreen) and Trend model (blue).

VWAP_FASTEC_Training

Model	MAE	RMSE	FIC(0.98)	FIC(0.90)	FIC(0.50)
FPCA DAspot	4.552	6.478	0.309	0.201	0.096
DAspot	4.595	6.709	–	–	–
FPCA RLact	4.818	6.723	0.289	0.188	0.089
FPCA RLmk	5.172	7.218	0.273	0.177	0.084
FPCA RLdiff	5.838	8.080	0.244	0.157	0.074
FPCA no	5.954	8.271	0.238	0.153	0.074
FASTEC DAspot	6.025	8.508	0.760	0.627	0.235
FASTEC RLact	6.100	8.587	0.737	0.605	0.224
FASTEC RLmk	6.161	8.677	0.728	0.595	0.221
FASTEC RLdiff	6.389	8.968	0.681	0.555	0.210
FASTEC no	6.403	8.991	0.682	0.555	0.213
Trend	6.935	9.598	–	–	–

Table 6: In-sample performance of FPCA and FASTEC models with lag order selection by BIC. Point forecasts evaluated by MAE and RMSE for $\tau = 0.50$. Interval forecasts evaluated by FIC.

VWAP_FPCA_Training VWAP_FASTEC_Training

performance the BIC selected models outperform those selected by AIC, which is in line with the findings of Shmueli (2010).

4.2.1 FPCA model

The naive benchmark represented by the DAspot, provides the lowest RMSE compared to all models. However, point forecasts from the FPCA DAspot model do not differ that much from the naive forecast and do further provide forecasts of distributional characteristics. Moreover, the RMSE is lower and the FIC(0.98) is higher compared to the train data. Reported RMSEs from the FPCA models in the test data are in general lower than in the train period. An exception is given by the deterministic trend forecast which exhibits a higher RMSE than in the train data. Additionally, all FPCA models perform in the test period better than the fundamental model by Pape et al. (2016) which reports a RMSE of 9.70 for the years 2012 and 2013. However, the test period in this thesis is the year 2016. So one has to be careful to compare the results with data from 2012 and 2013. The fact that the naive forecast performs as best predictor, indicates that the data generating process of the VWAP series has changed. A reason for this could be the increase of liquidity in the intraday market. Traded volumes at the EPEX Spot intraday market increased form from $1,810$ GWh in January 2014 (EPEX Spot 2014) to $2,983$ GWh in December 2016 (EPEX Spot 2017*b*). Both figures contain accumulated values for the German and Austrian market as well as intraday volumes regarding hourly and 15-minute contracts. Nevertheless, monthly trading volumes have increased by more than 50% within the observed period. Daily profiles for 2016-01-21 and 2016-01-22 are depicted to see an example how the expectile curves give information on the dispersion of the VWAPs in figure (13). In both cases, the forecasted expectile curves add valuable information compared to the forecasted trend component. While the forecasted tail expectiles span reasonable forecast intervals on the 2016-01-22, this is not the case on the previous day. Additionally, the price level on 21st January is quite high compared to the Trend forecast. Both, the VWAP and DA Spot series exhibits higher prices than the average on this day. Thus, in case of extreme prices, the conditional mean prognosis performs as a poor point forecast but also the estimated tail curves fail to give reasonable insights about the dispersion of the VWAP curve.

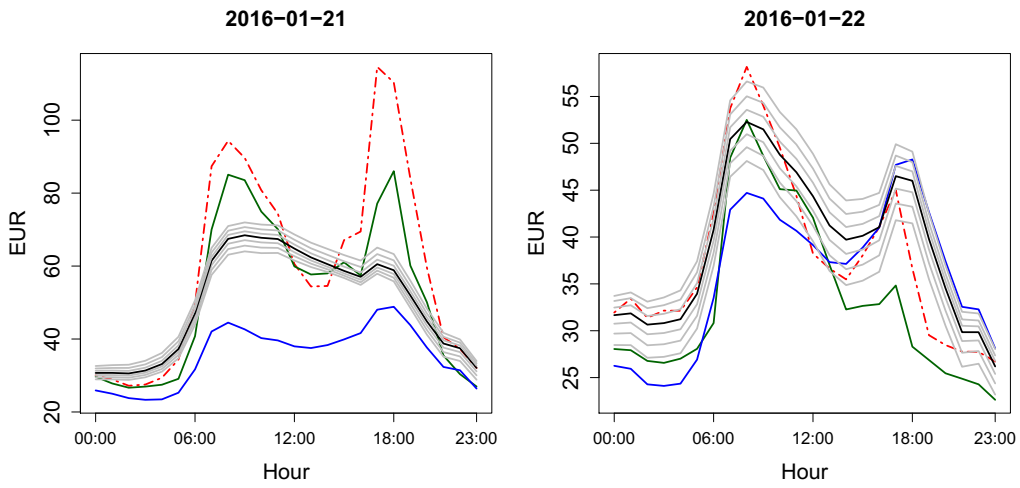

Figure 13: Actual VWAP curve (dashed red), curve forecasts for 50% expectile and for $\tau = 0.01, 0.05, 0.25, 0.75, 0.95, 0.99$ (grey) from FPCA DAspot, DAspot (darkreen) and Trend model (blue).

VWAP_FPCA_Forecast

4.2.2 FASTEC model

The reported RMSEs of the point forecasts obtained for $\tau = 0.50$ are higher for all FASTEC models compared to the in-sample period and the forecasts from the FPCA models. Nevertheless, the FIC is in all FASTEC models by far higher than those from the FPCA models. The FASTEC DAspot model provides with 78.40% an even higher $FIC(0.98)$ than within the train data. The dispersion of the forecasted VWAP by the FASTEC DAspot model is illustrated in figure (14). The interval forecast $\widehat{\pi}^{0.98}$ on 2016-01-21 fails to capture the high VWAPs during the morning and evening peak hours. On 2016-01-22 the forecasted intervals span a reasonable corridor for the VWAP movements.

4.2.3 Comparison of forecast performance

Forecasts are obtained with different approaches. The FPCA models produce forecasts for the 50% expectile, the FASTEC models aim at the conditional median. The Trend model takes only the deterministic trend into account and the DAspot model is available from the day-ahead auction. Thus, it makes sense to evaluate the quality of the model accuracy statistically with the Diebold-Mariano test (Diebold & Mariano 1995). This test is based on forecast errors and compares two competing forecasts. The null hypothesis is that the two forecasts have the same accuracy. The alternative hypothesis is that one forecast is superior

Model	MAE	RMSE	FIC(0.98)	FIC(0.90)	FIC(0.50)
DAspot	3.616	5.368	–	–	–
FPCA DAspot	3.882	5.785	0.328	0.216	0.109
FPCA RLact	4.842	7.087	0.252	0.162	0.075
FPCA RLmk	4.960	7.337	0.252	0.162	0.075
FPCA RLdiff	5.539	8.349	0.219	0.144	0.067
FPCA no	5.551	8.437	0.226	0.143	0.067
FASTEC DAspot	5.859	8.887	0.784	0.523	0.255
FASTEC RLact	6.118	9.256	0.704	0.451	0.215
FASTEC RLmk	6.172	9.322	0.693	0.454	0.217
FASTEC RLdiff	6.385	9.687	0.652	0.420	0.207
FASTEC no	6.396	9.702	0.677	0.441	0.214
Trend	7.068	10.494	–	–	–

Table 7: Out-of-sample performance with 730 days rolling window of FPCA and FASTEC models. Lag order selection by BIC. Point forecasts evaluated by MAE and RMSE for $\tau = 0.50$. Interval forecasts evaluated by FIC.

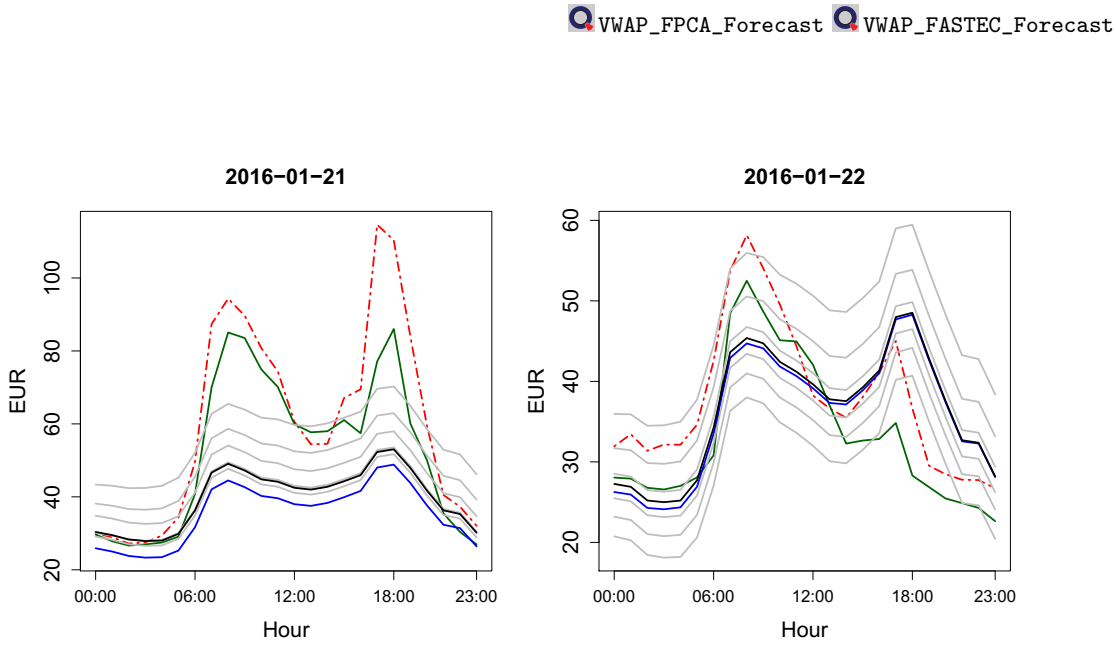

Figure 14: Actual VWAP curve (dashed red), curve forecasts for 50% quantile and for $\tau = 0.01, 0.05, 0.25, 0.75, 0.95, 0.99$ (grey) from FASTEC DAspot, DAspot (darkreen) and Trend model (blue).

VWAP_FASTEC_Forecast

to the other. The test has been conducted with the `R` package `forecast` by Hyndman & Khandakar (2008). Table (8) reports p-values (rounded to three decimal places) for the Diebold-Marino test. The test is conducted against the alternative hypothesis that the model given in the column is more accurate than the model in the row. The computed p-values are quite distinct and either very close to one or zero. The table can be interpreted in the following way. If the table reports a zero (i.e., rejects the null hypothesis significantly), the model in the column is more accurate than the model in the corresponding row. In case that the p-value is close to one, the null hypothesis is not rejected. The table confirms the results from table (7). The FPCA models outperform the FASTEC models in terms of RMSE. It is further confirmed that the DAspot is the best point forecast and also the most important explanatory variable.

In order to obtain deeper insights in the performance of the interval forecasts from FPCA DAspot and FASTEC DAspot are investigated in more detail. Therefore the FIC(0.98) is computed for every hour. The results are reported in table (9). Not surprisingly, the forecast intervals by FASTEC DAspot cover a higher proportion of observed VWAP than the FPCA DAspot in hour. While the FASTEC model reports higher FIC(0.98) during the off-peak hours, there is no clear distinction for the FPCA model. Further insights can be gained by looking at the size ω of the forecast intervals, which is computed for $\tau \in (0, 0.50)$ by

$$\omega_j^{1-2\tau}(t) = \widetilde{\widetilde{l}}_j^{1-\tau}(t) - \widetilde{\widetilde{l}}_j^{\tau}(t). \tag{43}$$

Considering the graphs in figure (13) and (14) it appears that the forecast intervals produced by FASTEC DAspot are longer than those from the FPCA DAspot. Since the reported RMSE of the FASTEC DAspot model is higher, it seems reasonable to have a look on the size of the forecasted intervals. The reason for such an investigation is that one could easily claim a very wide forecast interval that covers all observed VWAP. For example the interval $[-165.00, 145.00]$ would cover all VWAPs in the investigated data. However, such an interval would not help that much to get insights of future dispersion of VWAPs. For this reason, the distribution of the size $\omega^{0.98}$ is represented in the form of boxplots on hourly basis. Figure (15) shows the boxplots for the the interval size of the FPCA DAspot model and figure (15) represented the boxplots for the interval size of the FASTEC DAspot model.

One observes that the intervals from the FASTEC model are much wider in general for each hour. The size of the forecast intervals increase for both models until beginning of the peak hours. The median interval size for the FPCA model has a damped U shape during the

model	FPCA					FASTEC						
	DAspot	RLact	RLmk	RLdiff	no	DAspot	RLact	RLmk	RLdiff	no	DAspot	Trend
FPCA DAspot	–	1	1	1	1	1	1	1	1	1	0.001	1
FPCA RLact	0	–	1	1	1	1	1	1	1	1	0	1
FPCA RLmk	0	0	–	1	1	1	1	1	1	1	0	1
FPCA RLdiff	0	0	0	–	1	1	1	1	1	1	0	1
FPCA no	0	0	0	0	–	1	1	1	1	1	0	1
FASTEC DAspot	0	0	0	0	0	–	1	1	1	1	0	1
FASTEC RLact	0	0	0	0	0	0	–	1	1	1	0	1
FASTEC RLmk	0	0	0	0	0	0	0	–	1	1	0	1
FASTEC RLdiff	0	0	0	0	0	0	0	0	–	1	0	1
FASTEC no	0	0	0	0	0	0	0	0	0	–	0	1
DAspot	0.999	1	1	1	1	1	1	1	1	1	–	1
Trend	0	0	0	0	0	0	0	0	0	0	0	–

Table 8: P-values of the Diebold-Marino test against the alternative that model in column is more accurate than model in row. P-values are rounded to three digits. Forecast errors from point forecasts for ($\tau = 0.50$).

VWAP_Forecast_DM

peak hours and declines in the evening. However, the dispersion increases during peak hours until the 14:00 contract and then declines until midnight. Further the FPCA model reports interval sizes below zero. This refers to crossings of forecasted expectile curves. Those are observed for contracts between 12:00 and 18:00 as well as for contracts between 21:00 and 04:00. The median of $\omega^{0.98}$ from the FASTEC model increases until 16:00 and then declines. The outliers are difficult to interpret. For each hour an interval size of more than 30 EUR is reported. Even though the mean is not a robust statistical parameter, a comparison shows that mean and median are quite similar for FPCA DAspot, which is not the case for the FASTEC DAspot model. While FASTEC DAspot reports in more than 75% $\omega^{0.98} > 10.00$ EUR, forecasted intervals from the FPCA DAspot are rarely and only during some peak hours longer than 10.00 EUR. Since the standard deviation in the observed period is above 12.74 EUR, and forecasted intervals $\widehat{\pi}^{0.98}$ from the FASTEC DAspot model do never cross it is reasonable to conclude that the FASTEC DAspot model provides better forecast intervals.

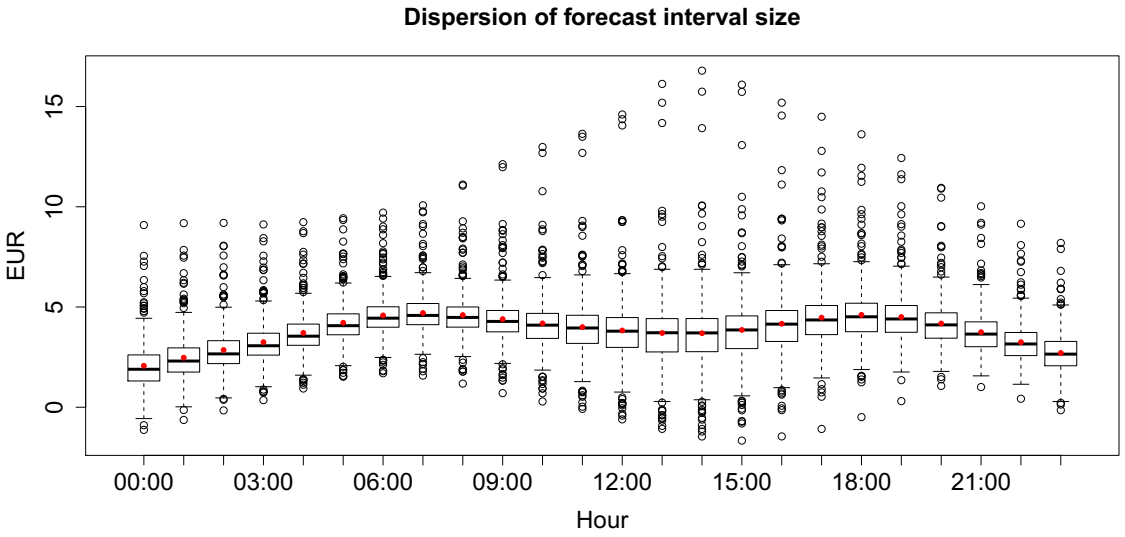

Figure 15: Density of forecast interval size $\omega^{0.98}$ from the FPCA DAspot model represented by boxplots for each hour. The box describes the IQR of $\omega^{0.98}$. The inner line is the median and the whiskers are given by 1.5×IQR. The red dot represents the mean of the interval size.

VWAP_FPCA_Forecast

	FIC(0.98) by	
Contract	*FPCA DAspot*	*FASTEC DAspot*
00:00	0.252	0.838
01:00	0.277	0.816
02:00	0.342	0.803
03:00	0.332	0.816
04:00	0.419	0.825
05:00	0.436	0.841
06:00	0.321	0.753
07:00	0.384	0.800
08:00	0.400	0.762
09:00	0.373	0.764
10:00	0.356	0.759
11:00	0.323	0.742
12:00	0.304	0.745
13:00	0.274	0.712
14:00	0.282	0.759
15:00	0.345	0.770
16:00	0.353	0.797
17:00	0.342	0.762
18:00	0.340	0.745
19:00	0.329	0.718
20:00	0.395	0.786
21:00	0.340	0.827
22:00	0.307	0.830
23:00	0.249	0.844

Table 9: FIC(0.98) by hour for FPCA DAspot and FASTEC DAspot.

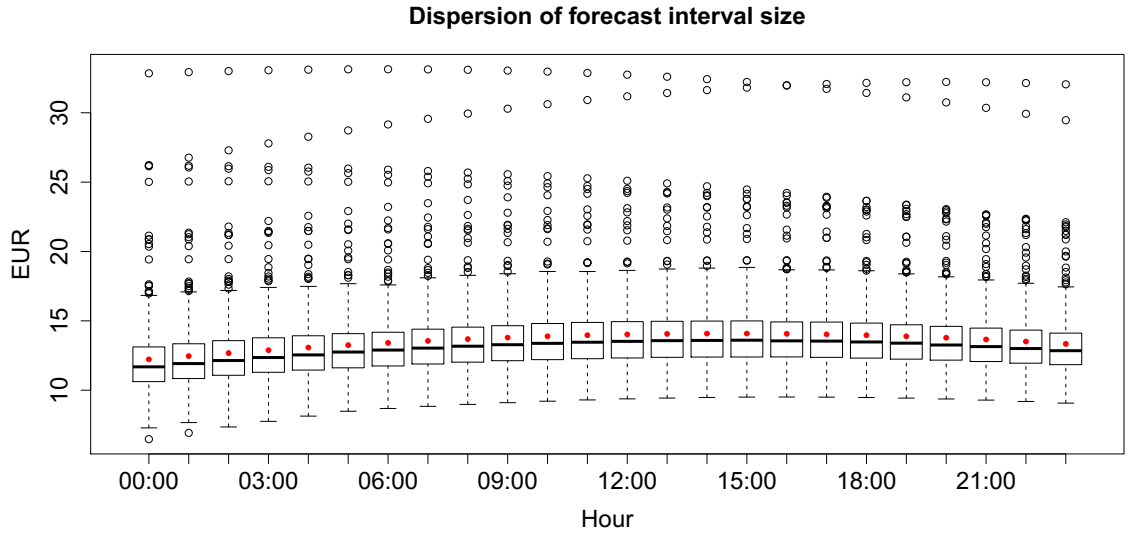

Figure 16: Density of forecast interval size $\omega^{0.98}$ from the FASTEC DAspot model represented by boxplots for each hour. The box describes the IQR of $\omega^{0.98}$. The inner line is the median and the whiskers are given by 1.5×IQR. The red dot represents the mean of the interval size.

`VWAP_FASTEC_Forecast`

5 Conclusion

The German intraday market provides a convenient design for traders and generators to adjust their short term portfolios. Especially the rise of intermittent renewable energy sources underlines the importance of intraday markets. This thesis investigates VWAPs from the continuous intraday trading at EPEX Spot. The application of two models based on functional data analysis and generalized quantile regression is presented. Probabilistic forecasts provide insights on the dispersion of future VWAPs that are important to producer and trader at the intraday market. Main risk factors of generalized quantile curves of the VWAPs are identified. Those factors are correlated with residual load and prices from the day-ahead market to produce probabilistic forecasts in terms of intervals. Those intervals could be used by market participants as a corridor for potential VWAP movements. The forecasted 98% intervals by the FASTEC model cover up to 78%, which is much more than those produced by the FPCA models which reaches at a max 33%.

It may be subject to further research to investigate how the forecasted intervals, especially in the case of the FASTEC model could be employed in trading strategies at the intraday market. In this context it should also investigate what size a reasonable forecast interval should be allowed to have in order to gain information that could be used by market partic-

ipants. Even though the forecast intervals from the FASTEC approach are wider, graphical illustrations show limited coverage of extreme prices. The analysis shows that prices from the day-ahead auction provide most important exogenous information among the functional data models. The analysis indicates that the dispersion of VWAP can be captured to some extent, but is far from perfect. It may be a topic for further research to investigate how extreme prices from the day-ahead auction could be exploited to improve interval forecasts of VWAP.

The model performance changes when point forecasts for VWAPs are considered. The applied techniques show that a part of the deseasonalized component can be explained. Both models add valuable information to the deterministic trend component. Most important exogenous information is the variation within the DAspot for the FPCA and FASTEC models during the train and test period. The rolling window out-of-sample forecast of the FPCA DAspot model provides with a RMSE of 5.785 the best point forecast among the applied models. Prices from the day-ahead auction provide with a RMSE of 5.368 even better point forecasts in the test period. This result is also confirmed with the Diebold-Marino test. Hence, if interest is only in point forecasts, using the prices from the day-ahead auction would be a cheap and reasonable figure. The fact that the RMSE from the DAspot as naive forecast and of the FPCA models is lower in the test period than in the train period indicates that the data generating process of the VWAP series has changed.

References

Aggarwal, S. K., Saini, L. & Kumar, A. (2009), 'Short term price forecasting in deregulated electricity markets: A review of statistical models and key issues', *International Journal of Energy Sector Management* **3**(4), 333–358.

Aigner, D. J., Amemiya, T. & Poirier, D. J. (1976), 'On the estimation of production frontiers: Maximum likelihood estimation of the parameters of a discontinuous density function', *International Economic Review* **17**(2), 377.

Amjady, N. & Hemmati, M. (2006), 'Energy price forecasting - problems and proposals for such predictions', *IEEE Power and Energy Magazine* **4**(2), 20–29.

Aneiros, G., Vilar, J. & Raña, P. (2016), 'Short-term forecast of daily curves of electricity demand and price', *International Journal of Electrical Power & Energy Systems* **80**, 96–108.

Antoch, J., Prchal, L., Rosa, M. R. D. & Sarda, P. (2010), 'Electricity consumption prediction with functional linear regression using spline estimators', *Journal of Applied Statistics* **37**(12), 2027–2041.

Aue, A., Norinho, D. D. & Hrmann, S. (2015), 'On the prediction of stationary functional time series', *Journal of the American Statistical Association* **110**(509), 378–392.

Beck, A. & Teboulle, M. (2009), 'A fast iterative shrinkage-thresholding algorithm for linear inverse problems', *SIAM Journal on Imaging Sciences* **2**(1), 183–202.

Bello, A., Reneses, J., Muñoz, A. & Delgadillo, A. (2016), 'Probabilistic forecasting of hourly electricity prices in the medium-term using spatial interpolation techniques', *International Journal of Forecasting* **32**(3), 966–980.

Belloni, A. & Chernozhukov, V. (2011), 'ℓ1-penalized quantile regression in high-dimensional sparse models', *The Annals of Statistics* **39**(1), 82–130.

BMWi (2017), 'Zeitreihen zur Entwicklung der erneuerbaren Energien in Deutschland'. Accessed 2017-04-15.
URL: *http://www.erneuerbare-energien.de/EE/Navigation/DE/Service/Erneuerbare_Energien_in_Zahlen/Zeitreihen/zeitreihen.html*

Bueno-Lorenzo, M., Àngeles Moreno, M. & Usaola, J. (2013), 'Analysis of the imbalance price scheme in the spanish electricity market: A wind power test case', *Energy Policy* **62**, 1010 – 1019.

Cabrera, B. L. & Schulz, F. (2016), Time-Adaptive Probabilistic Forecasts of Electricity Spot Prices with Application to Risk Management., SFB 649 Discussion Paper 2016-035, Sonderforschungsbereich 649, Humboldt Universität zu Berlin, Germany.

Cabrera, B. L. & Schulz, F. (in press), 'Forecasting generalized quantiles of electricity demand: A functional data approach', *Journal of the American Statistical Association* .

Chao, S.-K., Härdle, W. K. & Yuan, M. (2015), Factorisable Sparse Tail Event Curves, SFB 649 Discussion Paper 2015-034, Sonderforschungsbereich 649, Humboldt Universität zu Berlin, Germany.

Chao, S.-K., Härdle, W. K. & Yuan, M. (2016), Factorisable Multi-Task Quantile Regression, SFB 649 Discussion Paper 2016-057, Sonderforschungsbereich 649, Humboldt Universität zu Berlin, Germany.

Chen, X., Lin, Q., Kim, S., Carbonell, J. G. & Xing, E. P. (2012), 'Smoothing proximal gradient method for general structured sparse regression', *The Annals of Applied Statistics* **6**(2), 719–752.

Chen, Y. & Li, B. (2015), 'An adaptive functional autoregressive forecast model to predict electricity price curves', *Journal of Business & Economic Statistics* pp. 1–56.

Chernozhukov, V., Fernndez-Val, I. & Galichon, A. (2010), 'Quantile and probability curves without crossing', *Econometrica* **78**(3), 1093–1125.

Dette, H. & Volgushev, S. (2008), 'Non-crossing non-parametric estimates of quantile curves', *Journal of the Royal Statistical Society: Series B (Statistical Methodology)* **70**(3), 609–627.

Diebold, F. X. & Mariano, R. S. (1995), 'Comparing predictive accuracy', *Journal of Business & Economic Statistics* **13**(3), 253.

Eilers, P. H. C. & Marx, B. D. (1996), 'Flexible smoothing with B-splines and penalties', *Statistical Science* **11**(2), 89–121.

EPEX Spot (2014), 'Power trading results in January 2014', EPEX Spot press release.

EPEX Spot (2017*a*), 'Day-ahead-Auktion mit Lieferung in den deutschen/österreichischen Regelzonen'. Accessed 2017-04-15.
URL: *https://www.epexspot.com/en/product-info/auction/germany-austria*

EPEX Spot (2017*b*), 'EPEX Spot power trading results of December 2016', EPEX Spot press release.

EPEX Spot (2017*c*), 'Intraday market with delivery on the German TSO zone'. Accessed 2017-04-15.
URL: *https://www.epexspot.com/en/product-info/intradaycontinuous/germany*

Eubank, R. L. & Hsing, T. (2015), *Theoretical Foundations of Functional Data Analysis, with an Introduction to Linear Operators*, John Wiley and Sons Ltd.

Farahmand, H. & Doorman, G. (2012), 'Balancing market integration in the northern European continent', *Applied Energy* **96**, 316–326.

Ferraty, F. & Vieu, P. (2006), *Nonparametric Functional Data Analysis*, Springer New York.

Garnier, E. & Madlener, R. (2015), 'Balancing forecast errors in continuous-trade intraday markets', *Energy Systems* **6**(3), 361–388.

Gneiting, T. (2011), 'Quantiles as optimal point forecasts', *International Journal of Forecasting* **27**(2), 197–207.

Gooijer, J. G. D. & Hyndman, R. J. (2006), '25 years of time series forecasting', *International Journal of Forecasting* **22**(3), 443–473.

Greene, W. H. (2007), *Econometric Analysis*, Prentice Hall.

Hagemann, S. (2015), 'Price determinants in the German intraday market for electricity: An empirical analysis', *Journal of Energy Markets* **8**(2), 21–45.

Härdle, W. K. & Simar, L. (2015), *Applied Multivariate Statistical Analysis*, Springer.

Holttinen, H. (2005), 'Optimal electricity market for wind power', *Energy Policy* **33**(16), 2052–2063.

Hyndman, R. J. & Khandakar, Y. (2008), 'Automatic time series forecasting: The forecast package for R', *Journal of Statistical Software* **26**(3), 1–22.

Izenman, A. J. (1975), 'Reduced-rank regression for the multivariate linear model', *Journal of Multivariate Analysis* **5**(2), 248–264.

Jones, M. (1994), 'Expectiles and m-quantiles are quantiles', *Statistics & Probability Letters* **20**(2), 149–153.

Jónsson, T., Pinson, P., Madsen, H. & Nielsen, H. (2014), 'Predictive densities for day-ahead electricity prices using time-adaptive quantile regression', *Energies* **7**(9), 5523–5547.

Just, S. (2015), 'The German market for system reserve capacity and balancing', *SSRN Electronic Journal* .

Ketterer, J. C. (2014), 'The impact of wind power generation on the electricity price in germany', *Energy Economics* **44**, 270–280.

Kiesel, R. & Paraschiv, F. (2017), 'Econometric analysis of 15-minute intraday electricity prices', *Energy Economics* **64**, 77–90.

Koenker, R. (2005), *Quantile Regression (Econometric Society Monographs)*, Cambridge University Press.

Koenker, R. & Bassett, G. (1978), 'Regression quantiles', *Econometrica* **46**(1), 33.

Liebl, D. (2013), 'Modeling and forecasting electricity spot prices: A functional data perspective', *Ann. Appl. Stat.* **7**(3), 1562–1592.

Lütkepohl, H. (2005), *New introduction to multiple time series analysis*, Springer Science & Business Media.

Mayer, J. (2014), 'Electricity production and spot-prices in germany 2014', *Fraunhofer ISE, Freiberg, Germany* . Accessed 2017-04-25.
URL: *https://www.researchgate.net/publication/282654110_Electricity_Spot-Prices_in_-Germany_2014*

MKonline (2017), 'Time series for German electricity data', GONOGO database.
URL: *www.mkonline.com*

Moreira, R., Bessa, R. & Gama, J. (2016), Probabilistic forecasting of day-ahead electricity prices for the Iberian electricity market, *in* '2016 13th International Conference on the European Energy Market (EEM)', Institute of Electrical and Electronics Engineers (IEEE).

Mount, T. D., Ning, Y. & Cai, X. (2006), 'Predicting price spikes in electricity markets using a regime-switching model with time-varying parameters', *Energy Economics* **28**(1), 62–80.

Müsgens, F., Ockenfels, A. & Peek, M. (2014), 'Economics and design of balancing power markets in Germany', *International Journal of Electrical Power & Energy Systems* **55**, 392–401.

Nesterov, Y. (2005), 'Smooth minimization of non-smooth functions', *Mathematical Programming* **103**(1), 127–152.

Newey, W. K. & Powell, J. L. (1987), 'Asymmetric least squares estimation and testing', *Econometrica* **55**(4), 819.

Nicolosi, M. (2010), 'Wind power integration and power system flexibility - An empirical analysis of extreme events in Germany under the new negative price regime', *Energy Policy* **38**(11), 7257 – 7268. Energy Efficiency Policies and Strategies with regular papers.

Nowotarski, J. & Weron, R. (2015), 'Computing electricity spot price prediction intervals using quantile regression and forecast averaging', *Computational Statistics* **30**(3), 791–803.

Pape, C., Hagemann, S. & Weber, C. (2016), 'Are fundamentals enough? Explaining price variations in the German day-ahead and intraday power market', *Energy Economics* **54**, 376 – 387.

Ramsay, J. O. & Silverman, B. W. (2005), *Functional Data Analysis*, Springer-Verlag GmbH.

Ramsay, J. O., Wickham, H., Graves, S. & Hooker, G. (2014), *fda: Functional Data Analysis*. R package version 2.4.4.

Reinsel, G. C. & Velu, R. (1998), *Multivariate Reduced-Rank Regression*, Springer.

Riedel, S. & Weigt, H. (2007), German electricity reserve markets, Electricity Markets Working Papers WP-EM-20, Dresden University of Technology.

Rintamäki, T., Siddiqui, A. S. & Salo, A. (2017), 'Does renewable energy generation decrease the volatility of electricity prices? An analysis of Denmark and Germany', *Energy Economics* **62**, 270–282.

Rossi, G. D. & Harvey, A. (2009), 'Quantiles, expectiles and splines', *Journal of Econometrics* **152**(2), 179–185.

Schnabel, S. (2011), Expectile smoothing: New perspectives on asymmetric least squares. An application to life expectancy, PhD thesis, Utrecht University.

Schnabel, S. K. & Eilers, P. H. C. (2013), 'Simultaneous estimation of quantile curves using quantile sheets', *AStA Advances in Statistical Analysis* **97**(1), 77–87.

Serinaldi, F. (2011), 'Distributional modeling and short-term forecasting of electricity prices by generalized additive models for location, scale and shape', *Energy Economics* **33**(6), 1216–1226.

Shang, H. L. (2014), 'A survey of functional principal component analysis', *AStA Advances in Statistical Analysis* **98**(2), 121–142.

Shmueli, G. (2010), 'To explain or to predict?', *Statistical Science* **25**(3), 289–310.

Sobotka, F., Schnabel, S., Waltrup, L. S., Eilers, P., Kneib, T. & Kauermann, G. (2014), *expectreg: Expectile and Quantile Regression*. R package version 0.39.

Trapletti, A. & Hornik, K. (2016), *tseries: Time Series Analysis and Computational Finance*. R package version 0.10-35.

v. Selasinsky, A. (2016), The integration of renewable energy sources in continuous intraday markets for electricity, PhD thesis, Technische Universität Dresden.

Vilar, J. M., Cao, R. & Aneiros, G. (2012), 'Forecasting next-day electricity demand and price using nonparametric functional methods', *International Journal of Electrical Power & Energy Systems* **39**(1), 48–55.

Waltrup, L. S., Sobotka, F., Kneib, T. & Kauermann, G. (2015), 'Expectile and quantile regression—david and goliath?', *Statistical Modelling* **15**(5), 433–456.

Weron, R. (2006), *Modeling and Forecasting Electricity Loads and Prices: A Statistical Approach*, John Wiley & Sons.

Weron, R. (2014), 'Electricity price forecasting: A review of the state-of-the-art with a look into the future', *International Journal of Forecasting* **30**(4), 1030 – 1081.

Würzburg, K., Labandeira, X. & Linares, P. (2013), 'Renewable generation and electricity prices: Taking stock and new evidence for Germany and Austria', *Energy Economics* **40, Supplement 1**, S159 – S171. Supplement Issue: Fifth Atlantic Workshop in Energy and Environmental Economics.

Yao, Q. & Tong, H. (1996), 'Asymmetric least squares regression estimation: A nonparametric approach', *Journal of Nonparametric Statistics* **6**(2-3), 273–292.

Yuan, M., Ekici, A., Lu, Z. & Monteiro, R. (2007), 'Dimension reduction and coefficient estimation in multivariate linear regression', *Journal of the Royal Statistical Society: Series B (Statistical Methodology)* **69**(3), 329–346.

A Appendix

Categories for the impact of public holidays on electricity demand based on MKonline estimations. Category minor refers to an impact below $4,000$ Mwh, major refers to an impact of more than $9,000$ Mwh. Bridge day refers to days before and after a public holiday from category major when weekend a is connected. Saturday and Sunday refer to major holidays that take place on the respective weekend day. Special cases are the days before and after christmas. The period from 24th December to 1st January is treated as major public holiday, 22nd, 23rd of December and 2nd of January are treated as bridge days.

- Minor

  2014-01-06 2014-03-03 2014-03-04 2014-08-15 2014-10-31 2015-01-06 2015-02-16 2015-02-17 2016-01-06 2016-02-08 2016-02-09 2016-08-15 2016-10-31

- Major

  2014-01-01 2014-04-18 2014-04-21 2014-05-01 2014-05-29 2014-06-09 2014-06-19 2014-10-03 2014-12-24 2014-12-25 2014-12-26 2014-12-29 2014-12-30 2014-12-31 2015-01-01 2015-04-03 2015-04-06 2015-05-01 2015-05-14 2015-05-25 2015-06-04 2015-12-24 2015-12-25 2015-12-28 2015-12-29 2015-12-30 2015-12-31 2016-01-01 2016-03-25 2016-03-28 2016-05-05 2016-05-16 2016-05-26 2016-10-03 2016-11-01 2016-12-26 2016-12-27 2016-12-28 2016-12-29 2016-12-30

- Bridge day

  2014-01-02 2014-04-17 2014-04-22 2014-04-30 2014-05-02 2014-05-28 2014-05-30 2014-06-10 2014-06-18 2014-06-20 2014-10-02 2014-12-22 2014-12-23 2015-01-02 2015-04-02 2015-04-07 2015-04-30 2015-05-13 2015-05-15 2015-05-26 2015-06-03 2015-06-05 2015-10-02 2015-12-22 2015-12-23 2016-01-02 2016-03-24 2016-03-29 2016-05-02 2016-05-04 2016-05-06 2016-05-17 2016-05-25 2016-05-27 2016-10-04 2016-12-22 2016-12-23

- Saturday

  2014-04-19 2014-11-01 2014-12-27 2015-04-04 2015-10-03 2015-12-26 2016-03-26 2016-12-24 2016-12-31

- Sunday

  2014-04-20 2014-06-08 2014-12-28 2015-04-05 2015-05-24 2015-11-01 2015-12-27 2016-03-27 2016-05-01 2016-05-15 2016-12-25

B Tables

τ	λ
0.01	0.001101484
0.05	0.002353315
0.25	0.004636413
0.50	0.005355734
0.75	0.004635493
0.95	0.002348736
0.99	0.001099556

Table 10: Simulated λ for each τ-level.

VWAP_FASTEC_Training

Model	MAE	RMSE	FIC(0.98)	FIC(0.90)	FIC(0.50)
FPCA DAspot	4.544	6.450	0.310	0.201	0.097
FPCA RLact	4.792	6.666	0.287	0.187	0.091
DAspot	4.595	6.709	–	–	–
FPCA RLmk	5.149	7.172	0.273	0.177	0.084
FPCA RLdiff	5.838	8.080	0.246	0.159	0.074
FPCA no	5.954	8.271	0.238	0.154	0.074
FASTEC DAspot	6.025	8.508	0.760	0.626	0.235
FASTEC RLact	6.100	8.587	0.739	0.604	0.224
FASTEC RLmk	6.161	8.677	0.728	0.595	0.221
FASTEC RLdiff	6.389	8.968	0.683	0.556	0.210
FASTEC no	6.403	8.991	0.680	0.554	0.213
Trend	6.935	9.598	–	–	–

Table 11: In-sample performance of FPCA and FASTEC models with lag order selection by AIC. Point forecasts evaluated by MAE and RMSE for $\tau = 0.50$. Interval forecasts evaluated by FIC.

VWAP_FPCA_Training VWAP_FASTEC_Training

Model	MAE	RMSE	FIC(0.98)	FIC(0.90)	FIC(0.50)
DAspot	3.616	5.368	–	–	–
FPCA DAspot	3.915	5.820	0.325	0.213	0.104
FPCA RLact	4.866	7.105	0.247	0.158	0.075
FPCA RLmk	4.971	7.353	0.247	0.158	0.075
FPCA RLdiff	5.541	8.363	0.216	0.143	0.067
FPCA no	5.564	8.464	0.227	0.142	0.068
FASTEC DAspot	5.859	8.887	0.783	0.522	0.254
FASTEC RLact	6.119	9.257	0.698	0.451	0.213
FASTEC RLmk	6.173	9.322	0.685	0.454	0.215
FASTEC RLdiff	6.385	9.687	0.650	0.423	0.206
FASTEC no	6.396	9.702	0.672	0.440	0.214
Trend	7.068	10.494	–	–	–

Table 12: Out-of-sample performance with 730 days rolling window of FPCA and FASTEC models. Lag order selection by AIC. Point forecasts evaluated by MAE and RMSE for $\tau = 0.50$. Interval forecasts evaluated by FIC.

Model	MAE	RMSE	FIC(0.98)	FIC(0.90)	FIC(0.50)
DAspot -	3.616	5.368	–	–	–
FASTEC DAspot	4.373	6.616	0.743	0.545	0.317
FPCA DAspot	4.540	7.091	0.268	0.174	0.087
FPCA RLact	4.868	7.259	0.244	0.154	0.076
FASTEC RLact	4.800	7.371	0.725	0.528	0.299
FASTEC RLmk	4.984	7.580	0.690	0.511	0.293
FPCA RLmk	5.124	7.588	0.244	0.154	0.076
FASTEC RLdiff	5.637	8.639	0.639	0.458	0.246
FASTEC no	5.423	8.355	0.692	0.493	0.274
FPCA no	5.599	8.635	0.215	0.139	0.064
FPCA RLdiff	6.207	9.541	0.203	0.129	0.065
Trend -	7.068	10.494	–	–	–

Table 13: Out-of-sample performance with 60 days rolling window of FPCA and FASTEC models. Lag order selection by BIC. Point forecasts evaluated by MAE and RMSE for $\tau = 0.50$. Interval forecasts evaluated by FIC.

`VWAP_FPCA_Forecast` `VWAP_FASTEC_Forecast`

Model	MAE	RMSE	FIC(0.98)	FIC(0.90)	FIC(0.50)
DAspot	3.616	5.368	–	–	–
FASTEC DAspot	4.775	7.017	0.685	0.491	0.308
FASTEC RLact	4.869	7.442	0.695	0.484	0.271
FASTEC RLmk	5.085	7.715	0.671	0.478	0.268
FPCA DAspot	5.221	8.176	0.247	0.163	0.085
FPCA RLact	5.550	8.898	0.219	0.146	0.073
FASTEC no	5.587	8.604	0.680	0.466	0.261
FPCA RLmk	5.897	9.671	0.219	0.146	0.073
FASTEC RLdiff	6.437	9.762	0.596	0.394	0.205
FPCA no	6.465	11.517	0.211	0.133	0.065
Trend	7.068	10.494	–	–	–
FPCA RLdiff	7.878	12.625	0.188	0.131	0.066

Table 14: Out-of-sample performance with 30 days rolling window of FPCA and FASTEC models. Lag order selection by BIC. Point forecasts evaluated by MAE and RMSE for $\tau = 0.50$. Interval forecasts evaluated by FIC.

Declaration of Authorship

I hereby confirm that I have authored this Master's thesis independently and without use of others than the indicated sources. All passages which are literally or in general matter taken out of publications or other sources are marked as such.

Berlin, May 1, 2017

Johannes Stoiber